Utrecht University

Master's Thesis

Validating lipid biomarker-based sea surface temperature proxies $U^{k'}_{37}$ and TEX_{86} in the Mediterranean Sea

---

Daisy Bouwmans (6899935)

First supervisor: Francien Peterse
Second supervisor: Addison Rice

Graduation research (GEO4-1520)
45 ECTS

15/11/2022

Contents

Abstract 2
1. Introduction 3
2. Hydrographic Setting 7
3. Methods 8
3.1 Sediment trap 8
3.2 Biomarker analysis 9
3.2.1 Alkenone preparation, analysis and proxy calculation 9
3.2.2 IsoGDGT preparation, analysis and proxy calculation 10
4. Results 11
4.1 Satellite data 11
4.2 $U^{k'}_{37}$ SST estimates 11
4.3 TEX_{86} SST estimates 11
4.4 Alkenone fluxes 13
4.5 IsoGDGT fluxes 13
4.6 IsoGDGT ratios per depth 14
4.7 Correlation between isoGDGT ratios and TEX_{86} SSTs 17
4.7.1 [GDGT-2]/[GDGT-3] ratio versus TEX_{86} SSTs 17
4.7.2 [GDGT-0]/[Cren] ratio versus TEX_{86} SSTs 17
4.7.3 [Cren']/([Cren] + [Cren']) ratio versus TEX_{86} SSTs 18
5. Discussion 19
5.1 Underestimation of SSTs by the $U^{k'}_{37}$ index 19
5.2 Overestimation of SSTs by the TEX_{86} index 19
6. Conclusion 21
References 22
Appendix 1. $U^{k'}_{37}$ values and TEX_{86} values 33
Appendix 2. IsoGDGT values at the three depths 35
Appendix 3. P and R^2 values 38

Abstract

Sea surface temperature (SST) reconstructions based on lipid biomarker proxies $U^{k'}_{37}$ and TEX_{86} show offsets from expected values in the Mediterranean Sea compared to other parts of the global ocean. In surface sediments, SSTs based on $U^{k'}_{37}$ are often 2–4°C colder than mean annual values, whereas SSTs based on TEX_{86} are generally 2–6°C warmer. $U^{k'}_{37}$ is known to be prone to biases towards the production season of alkenones, a non-linear temperature response to temperatures >24°C and resuspension of alkenones when exported to the sea floor. TEX_{86}, on the other hand, can be biased by the input of isoGDGTs produced by non-Thaumarchaeota or Thaumarchaeota living in the deep sea. This study assesses sources of bias in these proxies in the Mediterranean Sea by using sediment traps moored in the Bannock Basin at 500 m, 1500 m and 2500 m depth, collecting alkenones and isoGDGTs in a near-continuous time serie between 2008 and 2011. The data show that SST estimates based on $U^{k'}_{37}$ underestimate mean annual values by 4°C in the upper trap and 6°C in the middle and lower trap. This colder bias is caused by the bias towards the production season of the alkenones, proved by the high alkenone fluxes in winter. SST estimates based on TEX_{86} overestimate mean annual values by 8-9°C at each sediment trap. This warmer bias is a result of isoGDGT contributions by Group I.1b Thaumarchaeota and deep-water dwelling Thaumarchaeota, proved by [Cren']/([Cren] + [Cren']) ratio values of >0.04 and the [GDGT-2]/[GDGT-3] ratio values of >5, respectively.

KEYWORDS:
$U^{k'}_{37}$, TEX_{86}, Mediterranean Sea, sea surface temperature, alkenone/isoGDGT fluxes

1. Introduction

Sea surface temperature (SST) is an important parameter to study climate variability, abrupt climate change and the impact of continually occurring events on local climates. SSTs are used to understand the link between oceans and the atmosphere, they provide information on the global climate system and are useful to study marine ecosystems. Instrumental records of SSTs merely span until 1850 (Kennedy et al., 2011) and complete instrumental records covering more than 100 years are sparse (Laepple and Huybers, 2014). To reconstruct SSTs over multidecadal and longer time scales, paleoclimate proxies are needed (Laepple and Huybers, 2014). Up till now, several organic geochemical proxies have been developed to reconstruct SSTs over longer time scales, including the $U^{k'}_{37}$-index (Prahl & Wakeman, 1987) and the TEX_{86}-index (Schouten et al., 2002).

The first paleothermometer studied in this thesis is the $U^{k'}_{37}$-index. This index is based on the concentrations of di- and tri-unsaturated ketones with 37 carbon atoms produced by haptophyte algae (Prahl & Wakeman, 1987) (Fig. 1). The algae are thought to produce more di-unsaturated C_{37} alkenones ($C_{37:2}$) relative to tri-unsaturated C_{37} alkenones ($C_{37:3}$) at higher growth temperatures (Brassell et al., 1986). Thus, high $C_{37:3}$ values are linked to lower SSTs and high $C_{37:2}$ values are related to higher SSTs. The linear relationship between the $U^{k'}_{37}$-index and sea surface temperatures is experimentally proved in culture studies of haptophyte species *Emiliania huxleyi* (Prahl et al., 1988; Herbert, 2001) and in global core-top calibrations (Müller et al., 1998; Conte et al., 2006). The $U^{k'}_{37}$-index is known to span till the Eocene period (Bianchi & Canuel, 2011; Schouten et al., 2013).

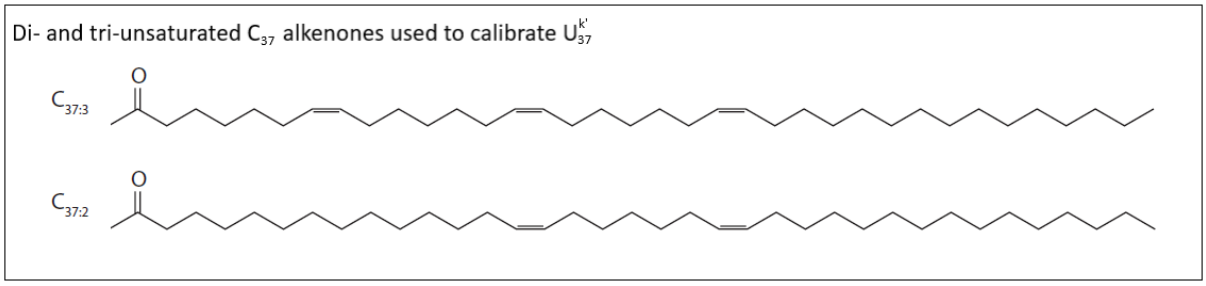

Fig. 1. Structures of C_{37} alkenones. Modified after Bianchi and Canuel (2011).

The second paleothermometer studied in this thesis is the TEX_{86}-index. This index is based on the relative abundance of isoprenoid Glycerol Dibiphytanyl Glycerol Tetraethers (isoGDGTs) consisting of 86 carbon atoms, largely produced by a group of marine archaea called Thaumarchaeota (Schouten et al., 2002). The isoGDGTs contain one to three cyclopentane moieties ([GDGT-1], [GDGT-2], [GDGT-3], respectively) or four cyclopentane moieties with

an additional cyclohexane moiety (Crenarchaeol stereoisomer or [Cren'])(Fig. 2). Schouten et al. (2002) designed TEX_{86} based on the relative abundance of isoGDGTs in marine surface sediments. [GDGT-0], with zero cyclopentane rings, and crenarchaeol, with four cyclopentane rings and one cyclohexane ring similar to crenarchaeol stereoisomer, are excluded from this equation (Fig. 2). The index is known to span till the Cretaceous period (Bianchi & Canuel, 2011; Schouten et al., 2013).

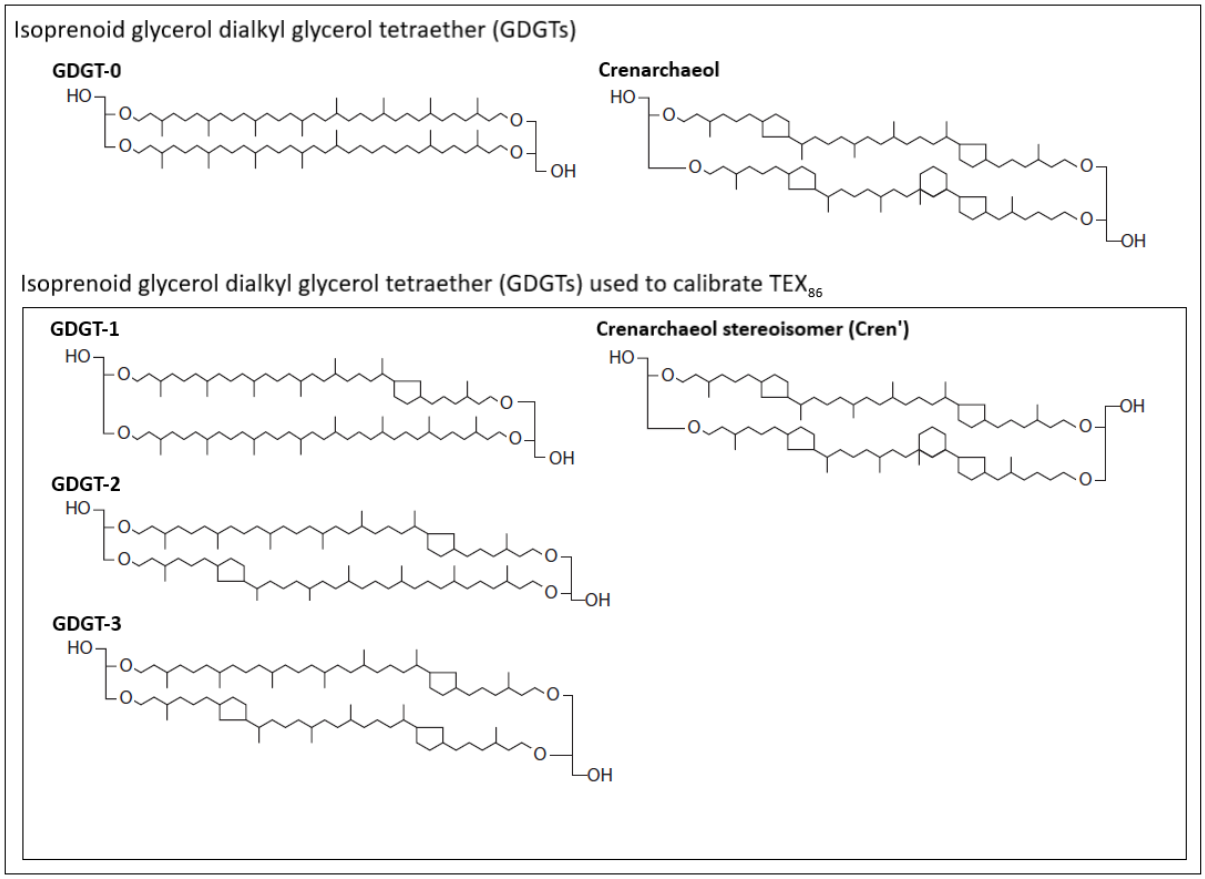

Fig. 2. Structures of the GDGT compounds. Modified after Bianchi and Canuel (2011).

Though both $U^{k'}_{37}$ and TEX_{86} have been applied in many studies, the validity of these proxies in the Mediterranean Sea is still heavily debated (De Lange et al., 1990; Ziveri et al., 1995; Ternois et al., 1996; Ternois et al., 1997; Sicre et al., 1999; Rutten et al., 2000; Ziveri et al., 2000; Rosell-Melé & Prahl, 2013; Kim et al., 2015; Tierney and Tingley, 2018; Besseling et al., 2019; Skampa et al., 2020; Morcillo-Montalbá et al., 2021; Rice et al., 2022).

In this region, SST estimates in surface sediments based on $U^{k'}_{37}$ are generally 2-4ºC colder than mean annual values (Tierney & Tingley, 2018). This underestimation might be explained by a number of possible biases. The flux of suspended material from haptophyte algae, which create C_{37} alkenones, is highly seasonal in the Mediterranean Sea (Ternois et al., 1996; Ziveri

et al., 1995; Sicre et al 1999; Triantaphyllou et al., 2004), creating a possible seasonal bias of the SST estimates. The calibration of the $U^{k'}_{37}$ index could also be biased towards non-linear temperature sensitivity at the low and high ends of the calibration range (Tierney and Tingley, 2018). The relationship between $U^{k'}_{37}$ and SST is only described well between 8ºC and 25ºC (Prahl et al., 1988), or 24ºC (Richey and Tierney, 2016). Above and below these threshold levels, the $U^{k'}_{37}$-index displays a non-linear relation to SSTs (Richey and Tierney, 2016). Another bias might be the sinking rates of alkenones. This could be influenced by particles remaining in suspension, causing a time difference between observed SST minima/maxima and $U^{k'}_{37}$ SST minima/maxima (Mollenhauer et al., 2015). Suspension most likely influences the seasonal signal over depth as well (Mollenhauer et al., 2015). Additionally, the $U^{k'}_{37}$-index could be prone to influences of current advection and subsequent lateral transport over long distances (Thomsen et al., 1998; Benthien and Müller, 2000; Ohkouchi et al., 2002; Rühlemann and Butzin, 2006; Fallet et al., 2011). A recent study on the eastern Mediterranean Sea proves that some particles may travel over long distances before burial (Rice et al., 2022). Nevertheless, the SST at the point of the particle's origin and at the point of burial are much alike (Rice et al., 2022), disqualifying the influence of lateral transport during sinking as a proxy bias.

SST estimates in surface sediments based on TEX_{86} are generally 2-6ºC warmer than mean annual values in the Mediterranean Sea (Kim et al., 2016). This overestimation might be explained by contribution of GDGTs by other producers. [GDGT-0] is produced by chemolithotrophic ammonia-oxidizing Thaumarchaeota (Sinninghe Damsté et al., 2012; Schouten et al., 2013; Elling et al., 2017; Bale et al., 2019), anaerobic methane-oxidizing archaea (Pancost et al., 2001; Schouten et al., 2001) and methanogenic Euryarchaeota (Schouten et al., 2013). The input of isoGDGTs from methanogens can be assessed by the [GDGT-0]/[Cren] ratio (Blaga et al., 2009; Bechtel et al., 2010), for which a ratio of >2 is indicative of a substantial contribution of [GDGT-0] produced by methanogenic Euryarchaeota. [Cren'] is produced in high abundance by ammonia-oxidizing Group I.1b Thaumarchaeota (Sinninghe Damsté et al., 2002). This bias is assessed by the [Cren']/([Cren] + [Cren']) or f[Cren'] ratio (O'Brien et al., 2017). Elevated levels of f[Cren'] are indicative for more input of soil-derived isoGDGTs produced by Group I.1b Thaumarchaeota compared to aquatically-derived isoGDGTs produced by Group I.1a Thaumarchaeota (Sinninghe Damsté et al., 2012). For lakes, an f[Cren'] of >0.04 indicates a substantial input of isoGDGTs produced by Group I.1b Thaumarchaeota (Baxter et al., 2021). A high abundace of [GDGT-2] is produced by deep-water dwelling Thaumarchaeota (Taylor et al., 2013). Several studies have suggested the [GDGT-2]/[GDGT-3] ratio to study the influence of deep-water dwelling Thaumarchaeota (Taylor et al., 2013; Hernández-Sánchez et al., 2014; Kim et al., 2016). A [GDGT-2]/[GDGT-3] ratio of >5 confirms a substantial influence of isoGDGTs produced by deep-water Thaumarchaeota (Taylor et al., 2013).

For this thesis, I assess both temporal and spatial changes in alkenones and isoGDGTs in sediment trap material collected between 2008 and 2011 at 500 m, 1500 m, and 2500 m water depth from the Bannock Basin in the eastern Mediterranean Sea (Fig. 3). The aim of this study is to examine the relationship between alkenones and isoGDGTs and how the related proxies compare to SST. Additionally, a focus is placed on the transfer of alkenones and isoGDGTs to the sea floor. To study this, I propose two research questions: 1) How are $U^{k'}_{37}$ and TEX_{86} related to SSTs in the Mediterranean Sea?, and 2) How are alkenones and isoGDGTs exported to the sea floor in the Mediterranean Sea?

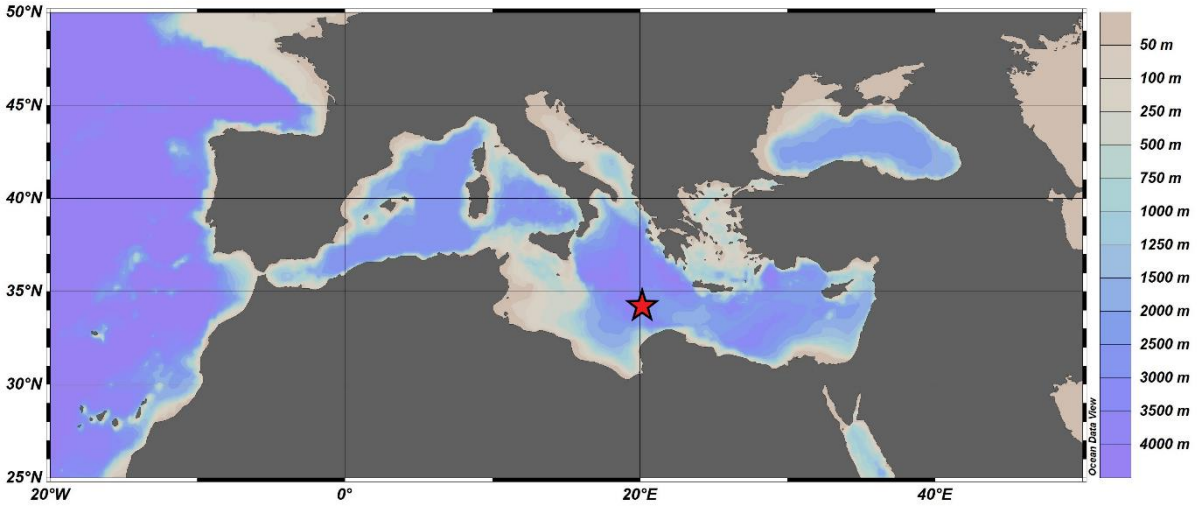

Fig. 3. Map of the Mediterranean Sea including sea floor depth and location of the sediment traps [red] (created with Ocean Data View)

2. Hydrographic Setting

The Mediterranean Sea is an enclosed basin connected to the Atlantic Ocean by the Strait of Gibraltar, which is divided in the Western Mediterranean sub-basin and the Eastern Mediterranean subbasin (Zavatarelli and Mellor, 1994)(Fig. 3). It is an oligotrophic area with isolated highly productive regions in the western basin (Ziveri et al., 1995). The Modified Atlantic Water (MAW) is found in the surface layer of both sub-basins and has a thickness of 50-200 m (Fig. 4) (Zavatarelli and Mellor, 1994). The surface flow is generally from west to east, causing colder and fresher water from the North Atlantic Ocean to enter the MAW from west to east as well (Roussenov et al., 1995). This direction is largely followed by temperature and salinity gradients, resulting in increasing surface temperature and salinity levels from west to east (Zavatarelli and Mellor, 1994). The Levantine Intermediate Water (LIW) is found in the subsurface waters of both sub-basins, between 200-800 m depth (Zavatarelli and Mellor, 1994). The LIW flows westward and follows an opposite flow direction compared to the MAW (Kim et al., 2016; Besseling et al., 2019). The former is characterized by temperatures ranging from 13ºC in the West to 15.5ºC in the East (Zavatarelli and Mellor, 1994). The Mediterranean Deep Water (MDW) is formed both in the Western Mediterranean sub-basin and the Eastern Mediterranean sub-basin, resulting in the West Mediterranean Deep Water (WMDW) and the East Mediterranean Deep Water (EMDW), respectively (Zavatarelli and Mellor, 1994). The WMDW is characterized by a temperature of 12.7ºC and the EMDW by a temperature of 13.6ºC (Zavatarelli and Mellor, 1994).

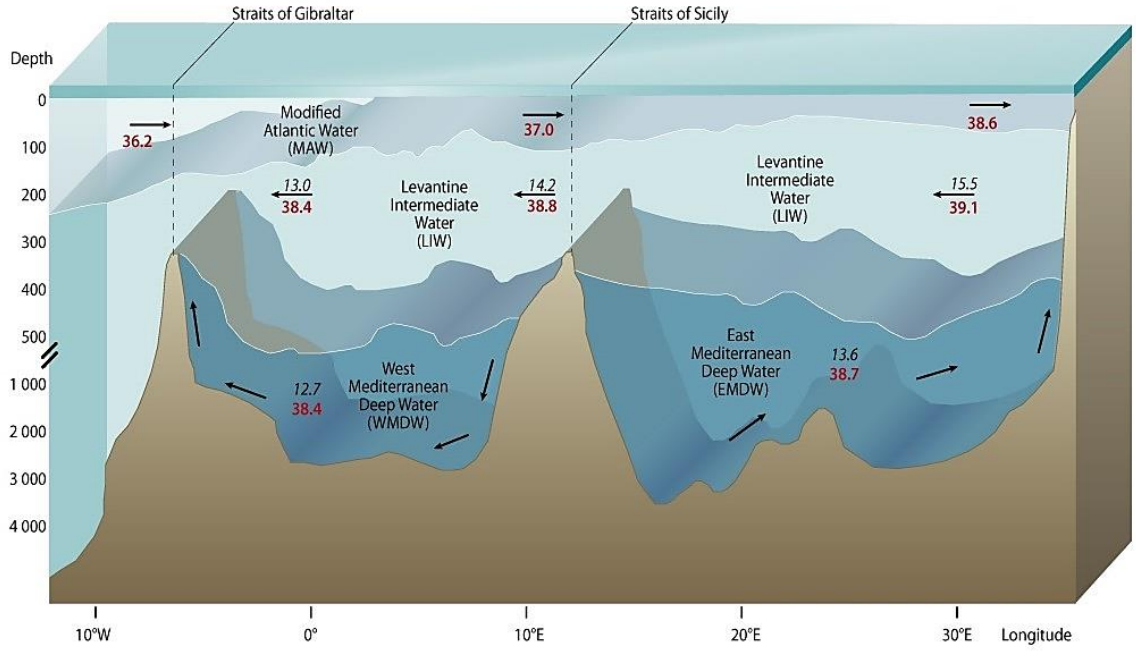

Fig. 4. Mediterranean water masses, including temperatures [black italic], levels of salinity [red bold] and flow direction [arrows]. Modified after State of the Mediterranean Marine and Coastal Environment (https://www.grida.no/resources/5885)

3. Methods

3.1 Sediment trap

Three Technicap PPS5/2 automated sediment traps were deployed in a time series in the southwestern Bannock Basin of the Mediterranean Sea (Libeccio subbasin: 34°18'N; 20°01'E) (Rutten et al., 2000; Ziveri et al., 2000) (Fig. 5). The traps are located well above the sea water/brine interface in oxygenated conditions (Rutten et al., 2000; Ziveri et al., 2000) at 545 m, 1750 m, and 2955 m water depth (Fig. 5; Table 1). Each trap is equipped with 24 collection cups, all mounted on a rotating plate programmed to rotate every 22 days and 12 hours (MP06ST) or 20 days and 20 hours (CP001ST). A time series deployment of 18 samples (MP06ST) and 24 samples (CP001ST) was collected in all traps over a near-continuous period of over 2.5 years. Sample 18 of the MP06ST mooring was opened for 6 days and still open upon retrieval. This sample was excluded from further analysis in this study.

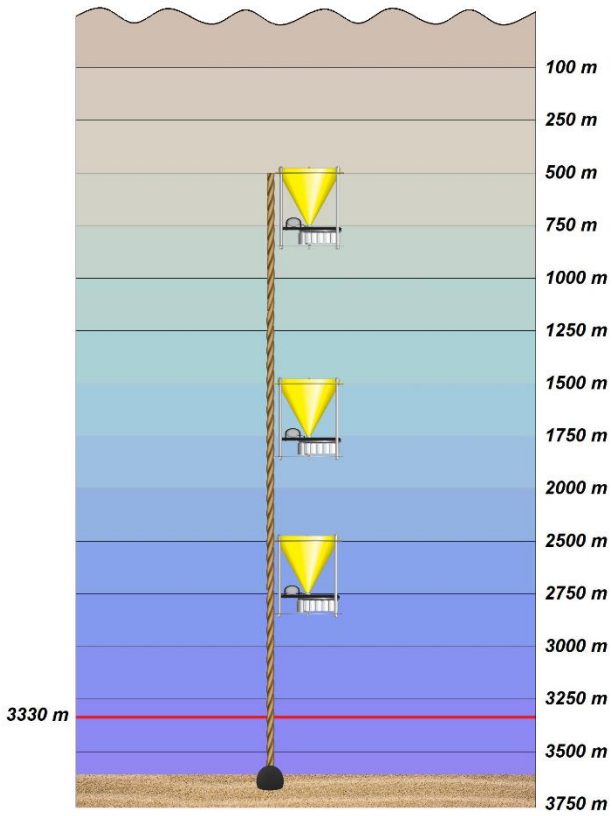

Fig. 5. Schematic view of the sediment trap depths, from top to bottom: 500 m, 1500 m and 2500 m. The water depth is 3530 m, and the seawater-brine interface is located at 3330 m depth [red line].

Table 1. Sediment trap details

Mooring phase	Start date	End date	Sample interval	Depth	Depth category
MP06ST4	07/11/2008	24/11/2009	22.5 days	545 m	500 m
MP06ST3	07/11/2008	24/11/2009	22.5 days	1750 m	1500 m
MP06ST2	07/11/2008	24/11/2009	22.5 days	2955 m	2500 m
CP001ST4	07/12/2009	21/04/2011	20.8 days	545 m	500 m
CP001ST3	07/12/2009	21/04/2011	20.8 days	1750 m	1500 m
CP001ST2	07/12/2009	21/04/2011	20.8 days	2955 m	2500 m

3.2 Biomarker analysis

Upon recovery of the traps , the samples were split into eight equal fractions using a pneumatic splitter (Tennant and Baker, 1992; Rutten et al., 2000). Seven fractions were filtered using a gas pressure system and divided into two groups: the first four were filtered on 0.2 μm glass fibre cellulose acetate filters, and the last three were filtered on 0.8 0 μm glass fibre filters. The swimmers were not removed. The remaining fraction was either filtered on a cellulose acetate filter or kept in solution. Upon arrival in the lab, the samples were freeze-dried, weighed, and extracted with a microwave MEX system (70ºC, 1.5 h), using 25 mL dichloromethane (DCM): methanol (MeOH) (9:1). The extract was evaporated to near dryness under N_2 using a TurboVap LV Caliper (32ºC, 1 kbar). The total lipid extract (TLE) was redissolved in 1-2 mL DCM:MeOH (9:1) and passed over a Pasteur pipette column containing 2cm of Na_2SO_4 using DCM:MeOH (9:1) as an eluent and dried under a stream of N_2. Acid hydrolysis of the TLE was performed by adding 0.5 mL 1.5N HCl in MeOH (27% 1:7) to the TLE vials and reacting in the oven (70ºC, 2h). Subsequently, liquid-liquid extraction was performed by the addition of 0.5 mL MilliQ and extracting with 4 mL DCM, drying it under a N_2 stream, and then eluting it over a Pasteur pipette column containing 2cm of Na_2SO_4 using DCM:MeOH (9:1) as an eluent. The dried sample then underwent methylation, for which 0.5 mL DCM:MeOH (1:1), 10 mL 0.2M diazomethane and 10 mL 0.2M acetic acid was added to each hydrolyzed sample before blow drying it under a stream of N_2. The samples were passed over a Pasteur pipette column containing 2 cm non-activated silica gel topped with Na_2SO_4 using ethyl acetate as an eluent and dried under a stream of N_2. The methylated samples were separated into apolar, neutral and polar fractions, eluting over a Pasteur pipette column containing 4 cm of AlOx using Hexane:DCM (9:1) as an eluent for apolar fractions, Hexane:DCM (1:1) as an eluent for neutral fractions and DCM:MeOH (1:1) as an eluent for polar fractions.

3.2.1 Alkenone preparation, analysis and proxy calculation

For quantitative analysis of alkenones, the neutral fractions were dissolved in 50 mL hexane (500 m trap) or 10 mL ethyl acetate (1500 m and 2500 m traps). Analyses were performed with a gas chromatograph-flame ionization detector (GC-FID) after manually co-injecting 1 mL dissolved sample and 1 mL squalene standard (63.8 mg/mL). The alkenone peaks were manually integrated in the chromatograms. These peaks were used to construct the $U_{37}^{k'}$ index as defined by Prahl and Wakeham (1987):

$$U_{37}^{k'} = \frac{[C_{37:2}]}{([C_{37:2}] + [C_{37:3}])}$$

The SSTs for the Bannock Basin were calculated by the global core top calibration (Prahl & Wakeman, 1988):

$$U_{37}^{k'} = 0.034 \cdot SST + 0.039$$

3.2.2 IsoGDGT preparation, analysis and proxy calculation

For quantitative analysis of the GDGTs, C_{46} GDGT 99ng/vial standard (CP001ST4 and CP001ST3) and C_{46} GDGT 152ng/vial standard (MP06ST4, MP06ST3, MP06ST2 and CP001ST2) was added to each sample before dissolving it in 500 mL (500 m trap) or 220 mL (1500 m and 2500 m trap) Hexane:IPA (99:1). The samples were then passed over a filter syringe before analyzing them with High-Performance Liquid Chromatography - Mass Spectrometry (HPLC-MS; Agilent Technologies 1290 Infinity equipped with an auto-injector and ChemStation chromatography manager software) by an autosampler. The GDGT peaks were manually integrated from the extracted ion current chromatograms of the $[M+H]^+$ ions. These peaks were used to construct the TEX^H_{86} as defined by Kim et al. (2015):

$$TEX_{86}^{H} = LOG\left(\frac{(GDGT-2)+(GDGT-3)+(Cren')}{(GDGT-1)+(GDGT-2)+(GDGT-3)+(Cren')}\right)$$

The SSTs for the Bannock Basin were calculated with the Mediterranean specific equation (Kim et al., 2015):

$$SST = 68.4 \cdot TEX_{86}^{H} + 38.6$$

4. Results

4.1 Satellite data

Throughout the period between November 2008 and April 2011, the satellite SSTs range between a minimum of 13.4ºC and a maximum of 28.5ºC (Fig. 6). The warmest months are towards the end of summer (August-September) and the coldest month is March. The annual mean temperature is ~21ºC.

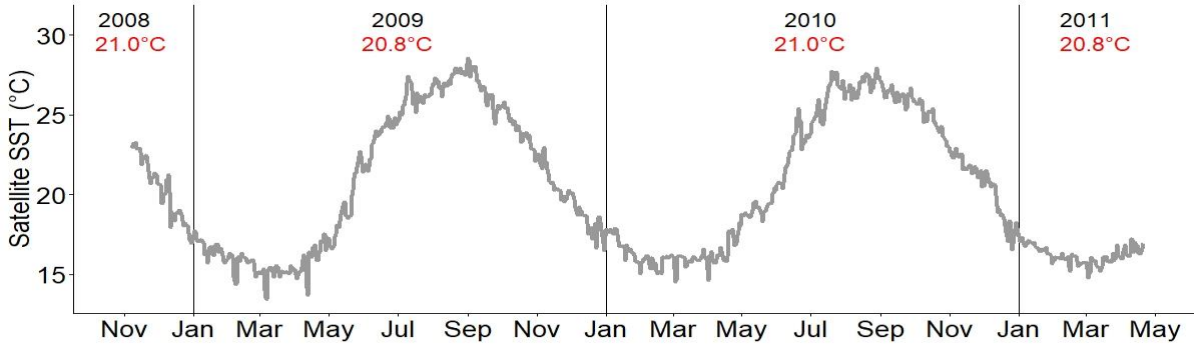

Fig. 6. Sea surface temperatures measured by satellites (grey) and annual mean sea surface temperatures (red).

4.2 $U^{k'}_{37}$ SST estimates

The $U^{k'}_{37}$ values are converted to SSTs and compared to satellite SSTs (Fig. 7). The $U^{k'}_{37}$ SSTs range between 11.4-27.6ºC, 11.1-23ºC, and 8.3-22.5ºC at the sediment trap depths of 500 m, 1500 m and 2500 m, respectively. The flux weighted averages give temperatures of 17.1ºC, 15.1ºC, and 15.1ºC from the upper to the lower trap. The SSTs display seasonality. However, due to a time lag, the timing of the SST maxima/minima differs per depth. From upper to lower, the SST maxima are in September/October, November/December, May/June. This is explained by a time lag of 1-2 months at 500 m depth, 5-6 months at 1500 m depth and 9 months at 2500 m depth. An exception to this seasonal signal are the first six months of 2009, when SSTs increase towards April and decrease again till July. This does not fit in with the patterns found in the other years at the same depth.

4.3 TEX_{86} SST estimates

The TEX_{86} values are converted to SSTs and compared to satellite SSTs (Fig. 8). The TEX_{86} SSTs range between 28.1-30.6ºC, 27.5-30.8ºC, and 28.6-31.0ºC at the sediment trap depths of 500 m, 1500 m and 2500 m, respectively. The flux weighted averages give temperatures of 29.4ºC, 29.7ºC, and 30.2ºC from the upper to the lower trap. The SSTs display seasonality, with highest temperatures in winter/spring (December-March), which is at least 4 months later than the maximum in satellite SSTs.

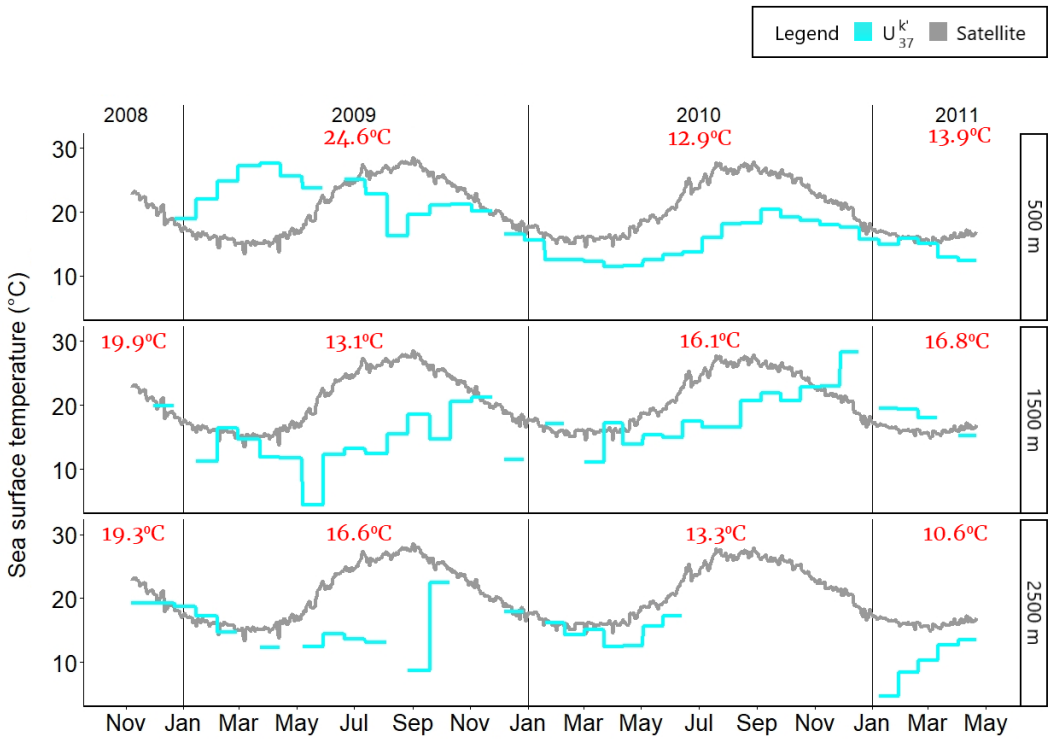

Fig. 7. Sea surface temperatures estimates by $U^{k'}_{37}$ (blue) and annual mean temperatures (red), compared with satellite measured SSTs (grey).

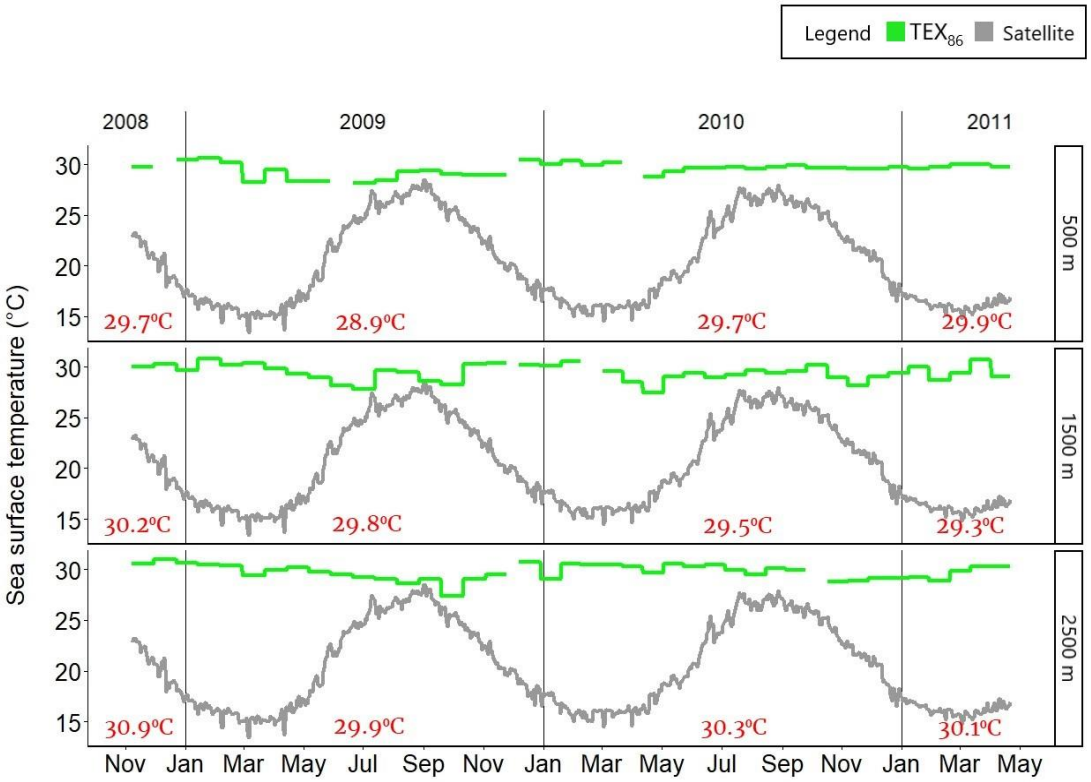

Fig. 8. Sea surface temperatures estimates by TEX_{86} (green) and annual mean temperatures (red), compared with satellite measured SSTs (grey).

4.4 Alkenone fluxes

$C_{37:3}$ and $C_{37:2}$ alkenones occur at the three trap deployment depths between 2008 and 2011 (Fig. 9). The alkenones are continuously exported throughout the year. The total C_{37} alkenone fluxes decrease over depth, ranging between 0.02 - 3.94, 0.004 - 0.681 and 0.001 - 0.15 µg/m^2/day from upper to lower trap, respectively, with an average flux of 0.47, 0.103 and 0.03 µg/m^2/day. The fluxes display seasonality, with higher fluxes towards winter/spring (December-May), accounting for up to 75% of the annual flux. The ratio between the $C_{37:3}$ and $C_{37:2}$ alkenones differs per depth. At 500 m, the fluxes are primarily made up of $C_{37:2}$ alkenones, except for the peak in the spring of 2010. At 1500 m depth, they often hold more $C_{37:3}$ alkenones than $C_{37:2}$ alkenones. At 2500 m, both $C_{37:3}$ alkenone fluxes and $C_{37:2}$ alkenone fluxes have comparable volumes.

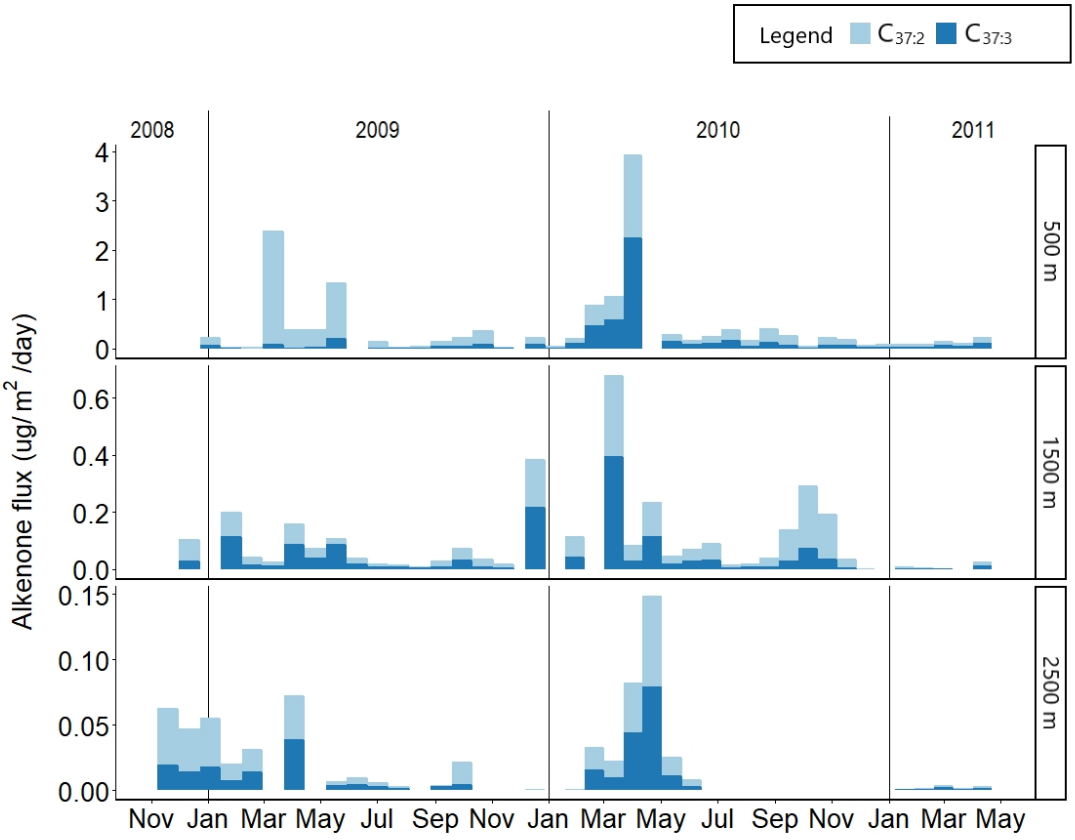

Fig. 9. Alkenone fluxes (µg/m2/day) at the three trap deployment depths.

4.5 IsoGDGT fluxes

Fluxes of [GDGT-0], [GDGT-1], [GDGT-2], [GDGT-3], Crenarchaeol ([Cren]) and Crenarchaeol Stereoisomer ([Cren']) are found at the three trap deployment depths between 2008 and 2011 (Fig. 10). The total isoGDGT flux decreases over depth, ranging between 42 - 1286, 5 - 1094 and 1.5 - 0.7 ng/m^2/day from upper to lower trap, respectively. There is no clear

seasonal signal which spans all depths. The composition of the fluxes differs over depth. At 500 m depth, The GDGT fluxes are primarily made up of [Cren] and [GDGT-0]. At 1500 m depth, the fluxes primarily hold [Cren]. At 2500 m depth, the fluxes are primarily composed of [Cren] and [GDGT-0].

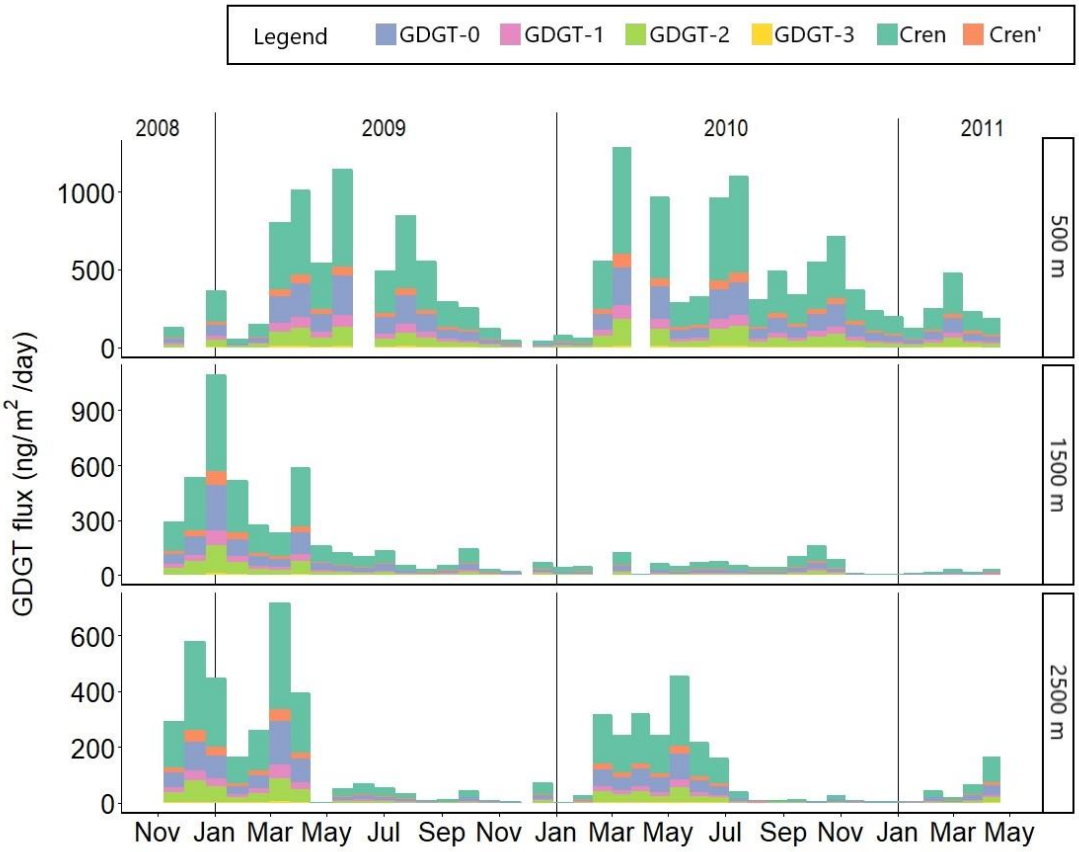

Fig. 10. IsoGDGT fluxes (ng/m2/day) at the three trap deployment depths.

4.6 IsoGDGT ratios per depth

The GDGT fluxes found between 2008 and 2011 are used to calculate the [GDGT-2]/[GDGT-3] ratio, the [GDGT-0]/[Cren] ratio and the [Cren']/([Cren]+[Cren']) ratio at each trap deployment depth (Fig. 11-13; Appendix 1,2). At 500 m depth (Fig. 10, Appendix 2), each ratio displays a seasonal signal. The [GDGT-2]/[GDGT-3] ratio ranges between 9.4 and 19.4, with the lowest values in spring (March-June) and the highest values in winter (December-January). The [GDGT-0]/[Cren] ratio ranges between 0.32 and 0.41. The highest values are found in spring (April-May) and the lowest values are found in winter (January-February). The [Cren']/([Cren]+[Cren']) ratio ranges between 0.08 and 0.11, with the highest values in winter (December-March) and the lowest values in summer (August-September).

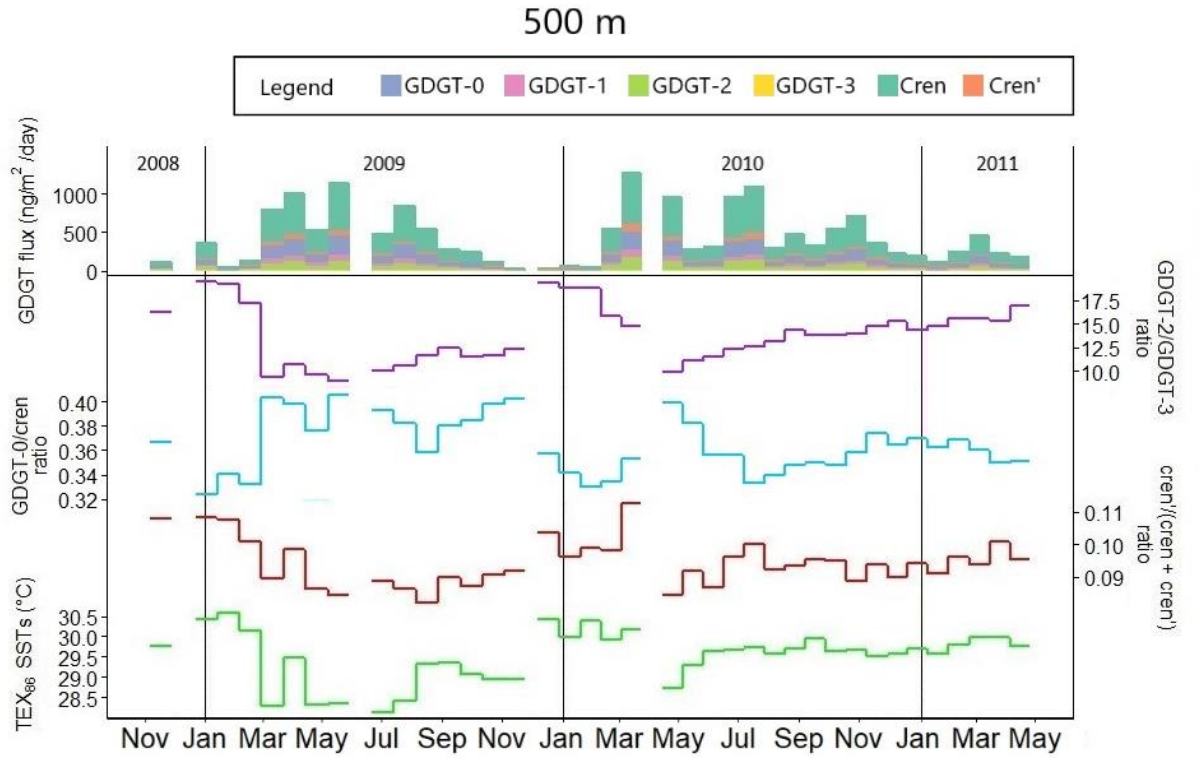

Fig. 11. Trap deployment depth 500 m, from top to bottom: isoGDGT fluxes, [GDGT-2]/[GDGT-3] ratio, [GDGT-0]/Cren ratio, [Cren']/(Cren+ [Cren']) ratio and TEX_{86} SSTs

At 1500 m depth (Fig. 12, Appendix 2), each ratio displays a seasonal signal, though clear seasonal trends are not always present. The [GDGT-2]/[GDGT-3] ratio ranges between 9 and 21 There is no clear trend visible in terms of high or low [GDGT-2]/[GDGT-3] ratio values. In December 2008, the values are low, while in December 2009, the values are extremely high. The [GDGT-0]/[Cren] ratio ranges between 0.3 and 0.5. This ratio seems to lack a seasonality signal as well. However, similar to the trend seen at 500 m depth, the [GDGT-0]/[Cren] ratio correlates negatively with the [GDGT-2]/[GDGT-3] ratio. The [Cren']/([Cren]+[Cren']) ratio ranges between 0.07 and 0.12, with the highest values in winter (December-March) and the lowest values in summer (August-September).

At 2500 m depth (Fig. 13), the [GDGT-2]/[GDGT-3] ratio ranges between 9.10 and 19.37. The [GDGT-0]/[Cren] ratio ranges between 0.32 and 0.61. The [Cren']/([Cren]+[Cren']) ratio ranges between 0.08 and 0.10. Although there are signs of seasonality in terms of the presence of minima and maxima in each ratio, there are no clear trends in this seasonal signal.

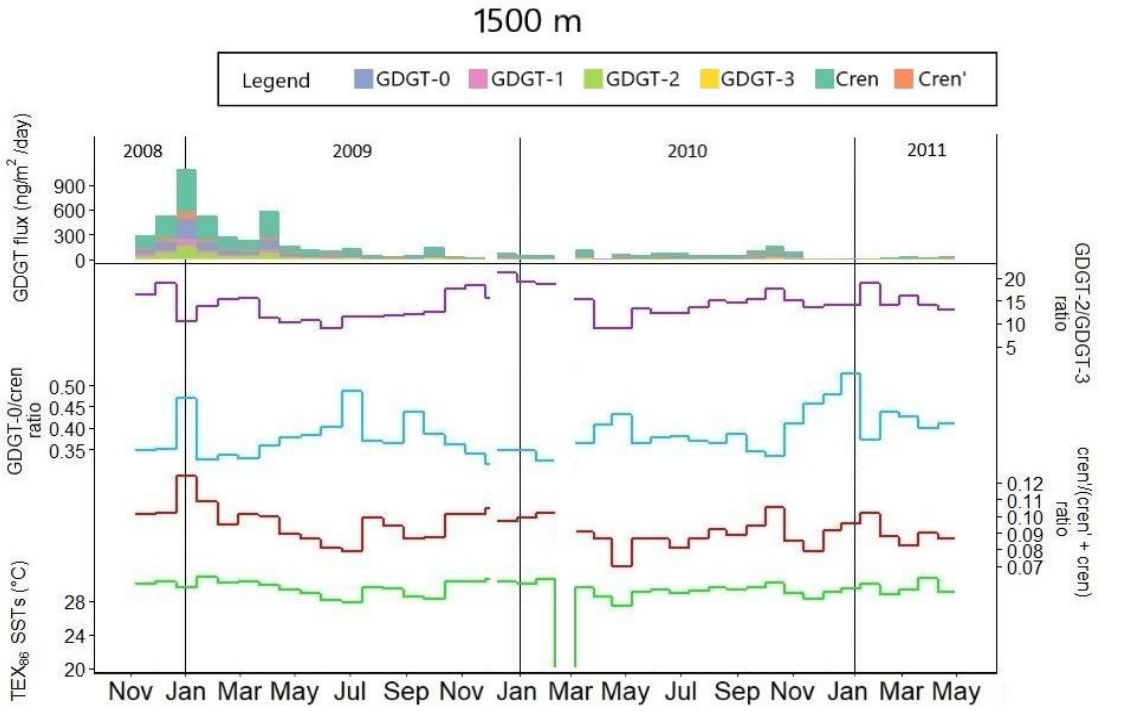

Fig. 12. Trap deployment depth 1500 m, from top to bottom: isoGDGT fluxes, [GDGT-2]/[GDGT-3] ratio, [GDGT-0]/Cren ratio, [Cren']/(Cren+ [Cren']) ratio and TEX_{86} SSTs

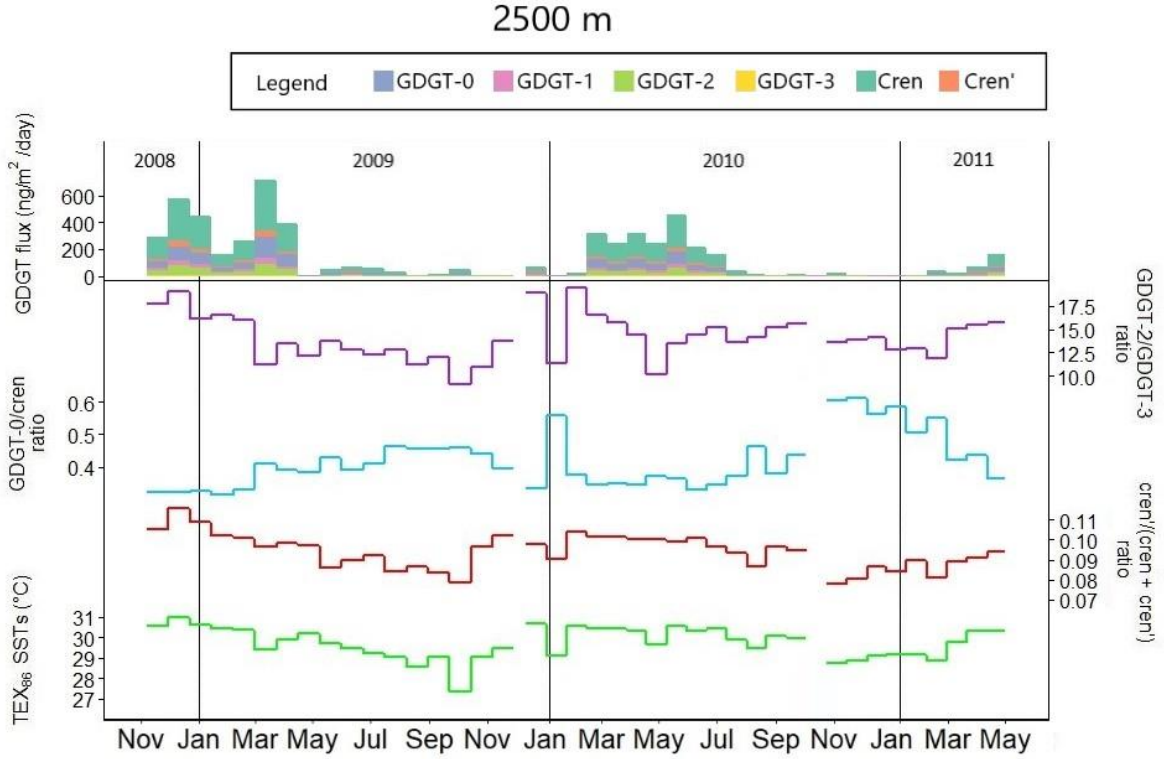

Fig. 13. Trap deployment depth 2500 m, from top to bottom: isoGDGT fluxes, [GDGT-2]/[GDGT-3] ratio, [GDGT-0]/Cren ratio, [Cren']/(Cren+ [Cren']) ratio and TEX_{86} SSTs

4.7 Correlation between isoGDGT ratios and TEX_{86} SSTs

The correlation between the influence of deep-water Thaumarchaeota, methanogens and Group I.1b soil Thaumarchaeota with TEX_{86} SSTs in studied by a plotting the TEX_{86} SSTs against [GDGT-2]/[GDGT-3] ratio, the [GDGT-0]/[Cren] ratio and [Cren']/([Cren]+[Cren']) ratio, respectively. Correlations are found significant at values of $P < 0.005$.

4.7.1 [GDGT-2]/[GDGT-3] ratio versus TEX_{86} SSTs

The [GDGT-2]/[GDGT-3] ratio correlates positively with the TEX_{86} SSTs (Fig. 14) at all sediment trap depths. This indicates that the input of isoGDGTs produced by deep-water Thaumarchaeota is related to SST overestimations by TEX_{86}.

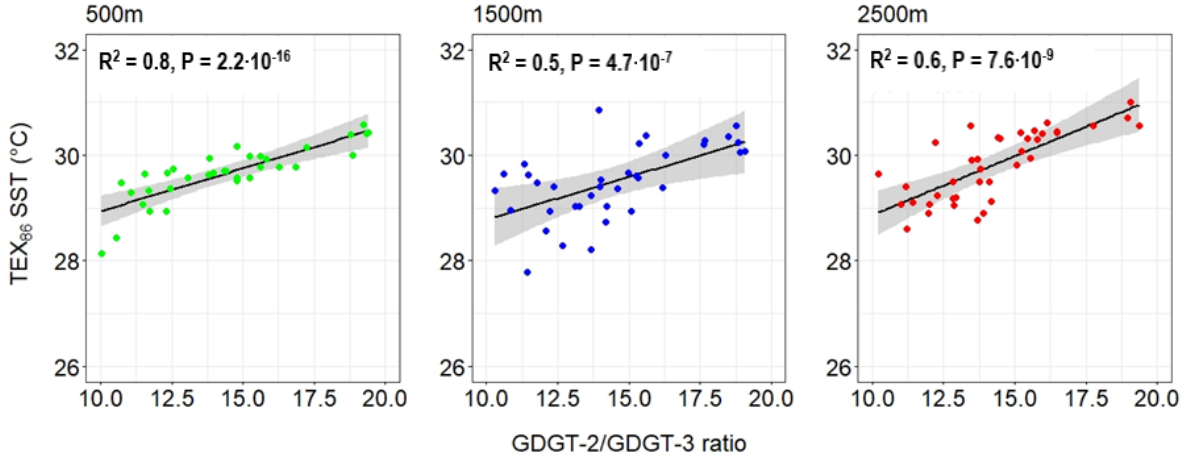

Fig. 14. [GDGT-2]/[GDGT-3] ratio versus TEX_{86} SST (ºC) at the three trap deployment depths.

4.7.2 [GDGT-0]/[Cren] ratio versus TEX_{86} SSTs

The [GDGT-0]/[Cren] ratio correlates negatively with the TEX_{86} SSTs (Fig. 15). This indicates that the input of isoGDGTs produced by methanogens is not related to SST overestimations by TEX_{86}, but instead enables a colder bias.

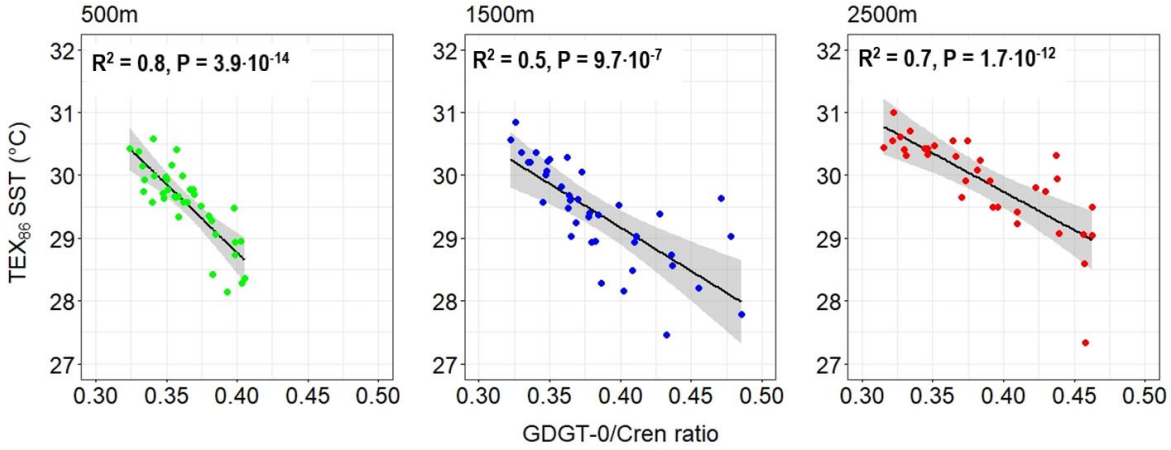

Fig. 15. [GDGT-0]/Cren ratio versus TEX_{86} SST (ºC) at the three trap deployment depths.

4.7.3 [Cren']/([Cren] + [Cren']) ratio versus TEX_{86} SSTs

The [Cren']/([Cren]+[Cren']) ratio correlates positively with the TEX_{86} SSTs (Fig. 16). This indicates that the input of isoGDGTs produced by soil-derived Group I.1b Thaumarchaeota is related to SST overestimations by TEX_{86}.

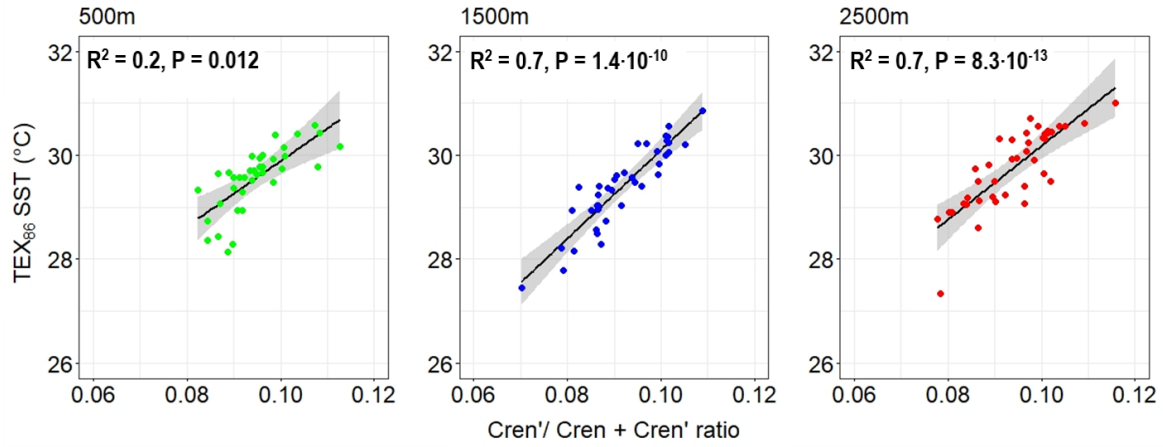

Fig. 16. [Cren']/Cren + [Cren'] ratio versus TEX_{86} SST (ºC) at the three trap deployment depths.

5. Discussion

5.1 Underestimation of SSTs by the $U^{k'}_{37}$ index

The reliability of SST estimates based on $U^{k'}_{37}$ is prone to influences of seasonality of the alkenone production (Tierney and Tingley, 2018). A winter-spring production might result in an underestimation of the $U^{k'}_{37}$ SSTs (Tierney and Tingley, 2018). The highest C_{37} alkenone flux in the Bannock Basin occurs in (late) winter and spring (December-May). This corresponds to winter-spring maxima of coccoliths observed in other sediment trap studies from the Eastern Mediterranean Sea (Malinverno et al., 2009; Skampa et al., 2020; Triantaphyllou et al., 2004) and in the Bannock Basin specifically (Ziveri et al., 1995; 2000). It is slightly different from the flux patterns found in the Western Mediterranean Sea, which have a major flux peak in fall (September-November) and a small peak in spring (May) (Ternois et al., 1996; 1997; Sicre et al., 1999). Additionally, another difference between the Bannock Basin and the Ligurian Sea (Western Mediterranean) is the number of annual flux peaks. The Ligurian Sea displays bi-annual peaks (Ternois et al., 1996; 1997; Sicre et al., 1999), while the Bannock Basin has only one flux peak per year. Export fluxes of coccolithophores found in the South-Western margin of Crete show an opposite trend to the one found in the Bannock Basin, with low overall export fluxes between November and February (Malinverno et al., 2009).

The SSTs based on $U^{k'}_{37}$ are indeed lower than the satellite SSTs. A comparison between the mean annual temperatures of the $U^{k'}_{37}$ estimates and the satellite data shows a difference of 4ºC at the 500 m trap and 6ºC at the 1500 m and 2500 m traps. The underestimation differs per season, with the largest difference in summer (5-7ºC) and the smallest differences in winter (2-4ºC). The highest alkenone fluxes are found in winter/spring as well. This explains the underestimation of $U^{k'}_{37}$, as its mean annual temperature is biased towards winter temperatures.

An exception to the aforementioned trends is the first six months of 2009 at the 500 m trap. Here, a seasonality is visible that is opposite to what is expected: an increase of SSTs towards April and a decrease towards August as a result of the input of more $C_{37:2}$ alkenones than $C_{37:3}$ alkenones. This trend is not repeated in other years or at the other depths. An explanation is the biosynthesis of more $C_{37:3}$ compared to $C_{37:2}$. This is likely as the flux of $C_{37:3}$ in this period is much lower than these fluxes in similar periods, i.e. the first six months of 2010.

5.2 Overestimation of SSTs by the TEX_{86} index

Several studies from the Mediterranean Sea have demonstrated that surface sediments at depths >1000m receive additional input of isoGDGTs from deep-water dwelling Thaumarchaeota (Kim et al., 2015; Besseling et al., 2019). Input from deep-water Thaumarchaeota is known to bias TEX_{86} SSTs to a higher value in the Mediterranean Sea (Besseling et al., 2019). Substantial

influence of deep-water Thaumarchaeota is assessed by [GDGT-2]/[GDGT-3] ratio values >5.0 (Taylor et al., 2013; Hernández-Sánchez et al., 2014, Rattanasriampaipong et al., 2022). In the Bannock Basin, the [GDGT-2]/[GDGT-3] ratio values are between 9 and 21 throughout the year for each depth, indicating a substantial contribution of deep-water dwelling Thaumarchaeota. Mean annual TEX_{86} estimates in this region indeed overestimate SSTs by 8-9ºC. Additionally, the influence of deep-water Thaumarchaeota is positively correlated with TEX_{86} SSTs. This further proves the ovestimation of TEX_{86} to be a result of the influence of deep-water Thaumarchaeota. Another source of isoGDGTs related to higher TEX_{86} SSTs is the input of soil-derived isoGDGTs produced by Group I.1b Thaumarchaeota (Weijers et al., 2006). A study from a small subtropical river-estuary system in China showed that sediment dominanted by marine input typically correspond to a [Cren']/([Cren]+[Cren']) ratio of <2 (Cheng et al., 2021). However, a study from a lake in East Africa proposes a threshold level of >0.04 as indicative for a substantial influence by Group I.1b Thaumarchaeota (Baxter et al., 2021). The [Cren']/([Cren]+[Cren']) ratios in the Bannock Basin range between 0.08 and 0.12 at each depth. This is both higher than 0.04 and lower than 2, indicating the substantial influence of soil-derived isoGDGTs on the TEX_{86} signal. This is further supported by the significant positive correlation found between the [Cren']/([Cren]+[Cren']) ratio and SSTs based on TEX_{86} at 1500m and 2500 m depth (Fig. 17). Interestingly, the correlation between the [Cren']/([Cren]+[Cren']) ratio and the SSTs based on TEX86 at 500 m depth are not correlated significantly, though the [Cren']/([Cren]+[Cren']) ratio lies well below 2. The reason behind this is unclear, though it should be noted that the relation between the [Cren']/([Cren]+[Cren']) ratio and the TEX86 SSTs would have been significant, if this study had deemed $P<0.5$ as significant instead of $P<0.005$.

The overestimation of TEX_{86} SSTs could also be explained the input of isoGDGTs produced by methanotrophic archaea (Zhang et al., 2020). The input of isoGDGTs from methanogens can be assessed by the [GDGT-0]/[Cren] ratio (Blaga et al., 2009; Bechtel et al., 2010). A [GDGT-0]/[Cren] ratio >2 indicates a substantial contribution of isoGDGTs produced by methanogens (Blaga et al., 2009; Bechtel et al., 2010, Sinninghe Damsté et al., 2012), instead of Thaumarchaeota. For a sediment trap study, the signal of methanogens will not be found, as these archaea are benthic. However, a positive relationship between the [GDGT-0]/[Cren] ratio and TEX_{86} SST could still be indicative for input of isoGDGTs produced by other archaea. This can be assessed by a sediment trap study. Nevertheless, in the Bannock Basin, this relationship is correlated negatively, excluding the input of other isoGDGT producing archaea.

6. Conclusion

To study the underestimation of SSTs by $U^{k'}_{37}$ and the overestimation of SSTs by TEX_{86} in the Mediterranean Sea, this thesis focussed on two research questions: 1) How are $U^{k'}_{37}$ and TEX_{86} related to SSTs?, and 2) How are alkenones and isoGDGTs exported to the sea floor? The data show that SST estimates based on $U^{k'}_{37}$ underestimate mean annual values by 4°C in the upper trap and 6°C in the middle and lower trap. This is due to the bias of this proxy towards winter temperatures. In contrast, SST estimates based on TEX_{86} overestimate mean annual values by 8-9°C at each sediment trap. This is explained by the input of soil-derived isoGDGTs produced by Group I.1b Thaumarchaeota, following [Cren']/([Cren]+[Cren'] ratio values of >0.04. It is further proved by the very small seasonal signal. Neither SST estimates based on $U^{k'}_{37}$, nor based on TEX_{86} are an accurate reflection of annual mean temperatures in the Eastern Mediterranean Sea. Both the alkenones and isoGDGTs are exported throughout the year. Though isoGDGTs do not display a seasonal bias, the alkenones show a higher flux towards their production season in winter/spring. Another difference is the source of the biomarkers. The alkenones are all exported from the surface waters to the sea floor, while the isoGDGT fluxes are influenced by input of isoGDGTs produced in the deep water, as proved by the [GDGT-2]/[GDGT-3] ratio value of >5.

References

Ausín, B., Haghipour, N., Bruni, E., & Eglinton, T. (2022). The influence of lateral transport on sedimentary alkenone paleoproxy signals. *Biogeosciences*, *19*(3), 613–627. https://doi.org/10.5194/bg-19-613-2022

Bale, N. J., Palatinszky, M., Rijpstra, W. I. C., Herbold, C. W., Wagner, M., & Sinninghe Damsté, J. S. (2019). Membrane Lipid Composition of the Moderately Thermophilic Ammonia-Oxidizing Archaeon "*Candidatus* Nitrosotenuis uzonensis" at Different Growth Temperatures. *Applied and Environmental Microbiology*, *85*(20). https://doi.org/10.1128/aem.01332-19

Basse, A., Zhu, C., Versteegh, G. J., Fischer, G., Hinrichs, K. U., & Mollenhauer, G. (2014). Distribution of intact and core tetraether lipids in water column profiles of suspended particulate matter off Cape Blanc, NW Africa. *Organic Geochemistry*, *72*, 1–13. https://doi.org/10.1016/j.orggeochem.2014.04.007

Baxter, A., van Bree, L., Peterse, F., Hopmans, E., Villanueva, L., Verschuren, D., & Sinninghe Damsté, J. (2021). Seasonal and multi-annual variation in the abundance of isoprenoid GDGT membrane lipids and their producers in the water column of a meromictic equatorial crater lake (Lake Chala, East Africa). *Quaternary Science Reviews*, *273*, 107263. https://doi.org/10.1016/j.quascirev.2021.107263

Bechtel, A., Smittenberg, R. H., Bernasconi, S. M., & Schubert, C. J. (2010). Distribution of branched and isoprenoid tetraether lipids in an oligotrophic and a eutrophic Swiss lake: Insights into sources and GDGT-based proxies. *Organic Geochemistry*, *41*(8), 822–832. https://doi.org/10.1016/j.orggeochem.2010.04.022

Besseling, M. A., Hopmans, E. C., Koenen, M., van der Meer, M. T., Vreugdenhil, S., Schouten, S., Sinninghe Damsté, J. S., & Villanueva, L. (2019). Depth-related differences in archaeal populations impact the isoprenoid tetraether lipid composition of the Mediterranean Sea water column. *Organic Geochemistry*, *135*, 16–31. https://doi.org/10.1016/j.orggeochem.2019.06.008

Bianchi, T. S., & Canuel, E. A. (2011). *Chemical Biomarkers in Aquatic Ecosystems* (1st ed.). Princeton University Press.

Blaga, C. I., Reichart, G. J., Heiri, O., & Sinninghe Damsté, J. S. (2009). Tetraether membrane lipid distributions in water-column particulate matter and sediments: a study of 47 European lakes along a north–south transect. *Journal of Paleolimnology*, *41*(3), 523–540. https://doi.org/10.1007/s10933-008-9242-2

Brassell, S. C., Eglinton, G., Marlowe, I. T., Pflaumann, U., & Sarnthein, M. (1986). Molecular stratigraphy: a new tool for climatic assessment. *Nature*, *320*(6058), 129–133. https://doi.org/10.1038/320129a0

Buckles, L. K., Verschuren, D., Weijers, J. W. H., Cocquyt, C., Blaauw, M., & Sinninghe Damsté, J. S. (2016). Interannual and (multi-)decadal variability in the sedimentary BIT index of Lake Challa, East Africa, over the past 2200 years: assessment of the precipitation proxy. *Climate of the Past*, *12*(5), 1243–1262. https://doi.org/10.5194/cp-12-1243-2016

Camerlenghi, A. (1988). *Subsurface dissolution of evaporites in the Eastern Mediterranean Sea* [MS Thesis]. Texas A&M University, College Station.

Camerlenghi, A., & Cita, M. B. (1987). Setting and tectonic evolution of some Eastern Mediterranean deep-sea basins. *Marine Geology*, *75*, 31–56.

Camerlenghi, A., & McCoy, F. W. (1990). Physiography and structure of Bacino Bannock (eastern mediterranean). *Geo-Marine Letters*, *10*(1), 23–30. https://doi.org/10.1007/bf02431018

Cheng, Z., Yu, F., Ruan, X., Cheng, P., Chen, N., Tao, S., Zong, Y., Yang, H., & Huang, Z. (2021a). GDGTs as indicators for organic-matter sources in a small subtropical river-estuary system. *Organic Geochemistry*, *153*, 104180. https://doi.org/10.1016/j.orggeochem.2021.104180

Cheng, Z., Yu, F., Ruan, X., Cheng, P., Chen, N., Tao, S., Zong, Y., Yang, H., & Huang, Z. (2021b). GDGTs as indicators for organic-matter sources in a small subtropical river-estuary system. *Organic Geochemistry*, *153*, 104180. https://doi.org/10.1016/j.orggeochem.2021.104180

Cita, M. B., Aghib, F., Malinverno, P., Mccoy, F., Nosetto, A., Parisi, E., Spezzibottani, G., Cambi, A., Camerlenghi, A., Corselli, C., Erba, E., Giambastiani, M., Herbert, T., Kastens, K. A., & Leoni, C. (1986). Precipitazione attuale di gesso in un bacino anossico profondo: prime osservazioni geologiche, idrologicbe, paleontologiche sul Bacino Bannock (Mediterraneo Orientale). *Giornale Di Geologia*, *47*(1–2), 143–163.

Cita, M. B., Fornaciari, M., Camerlenghi, A., Corselli, C., Erba, E., Mccoy, F. W., & Vezzoli, L. (1986). Anoxic basins of the eastern Mediterranean : New evidence from the Bacino Bannock area. *Memorie Della Societa Geologica Italiana*, *36*, 131–144.

Conte, M. H., Sicre, M. A., Rühlemann, C., Weber, J. C., Schulte, S., Schulz-Bull, D., & Blanz, T. (2006). Global temperature calibration of the alkenone unsaturation index ($U^{K'}_{37}$) in surface waters and comparison with surface sediments. *Geochemistry, Geophysics, Geosystems*, *7*(2), n/a-n/a. https://doi.org/10.1029/2005gc001054

Damsté, J. S., Schouten, S., Hopmans, E. C., van Duin, A. C., & Geenevasen, J. A. (2002). Crenarchaeol. *Journal of Lipid Research*, *43*(10), 1641–1651. https://doi.org/10.1194/jlr.m200148-jlr200

De Lange, G., Catalano, G., Klinkhammer, G., & Luther, G. (1990). The interface between oxic seawater and the anoxic Bannock brine; its sharpness and the consequences for the redox-related cycling of Mn and Ba. *Marine Chemistry*, *31*(1–3), 205–217. https://doi.org/10.1016/0304-4203(90)90039-f

De Lange, G., Middelburg, J., Van der Weijden, C., Catalano, G., Luther, G., Hydes, D., Woittiez, J., & Klinkhammer, G. (1990). Composition of anoxic hypersaline brines in the Tyro and Bannock Basins, eastern Mediterranean. *Marine Chemistry*, *31*(1–3), 63–88. https://doi.org/10.1016/0304-4203(90)90031-7

Dimiza, M. D., Triantaphyllou, M. V., Malinverno, E., Psarra, S., Karatsolis, B. T., Mara, P., Lagaria, A., & Gogou, A. (2016). The composition and distribution of living coccolithophores in the Aegean Sea (NE Mediterranean). *Micropaleontology*, *61*(6), 521–540. https://doi.org/10.47894/mpal.61.6.09

Elderfield, H. (2006). The Oceans and Marine Geochemistry: Treatise on Geochemistry, Volume 6 (1st ed.). Pergamon.

Evershed, R. P., Heron, C., & Goad, L. J. (1990). Analysis of organic residues of archaeological origin by high-temperature gas chromatography and gas chromatography-mass spectrometry. *The Analyst*, *115*(10), 1339. https://doi.org/10.1039/an9901501339

Fallet, U., Castañeda, I. S., Henry-Edwards, A., Richter, T. O., Boer, W., Schouten, S., & Brummer, G. J. (2012). Sedimentation and burial of organic and inorganic temperature proxies

in the Mozambique Channel, SW Indian Ocean. *Deep Sea Research Part I: Oceanographic Research Papers*, *59*, 37–53. https://doi.org/10.1016/j.dsr.2011.10.002

Fallet, U., Ullgren, J. E., Castañeda, I. S., van Aken, H. M., Schouten, S., Ridderinkhof, H., & Brummer, G. J. A. (2011). Contrasting variability in foraminiferal and organic paleotemperature proxies in sedimenting particles of the Mozambique Channel (SW Indian Ocean). *Geochimica Et Cosmochimica Acta*, *75*(20), 5834–5848. https://doi.org/10.1016/j.gca.2011.08.009

Gliozzi, A., Paoli, G., De Rosa, M., & Gambacorta, A. (1983). Effect of isoprenoid cyclization on the transition temperature of lipids in thermophilic archaebacteria. *Biochimica Et Biophysica Acta (BBA) - Biomembranes*, *735*(2), 234–242. https://doi.org/10.1016/0005-2736(83)90298-5

Guo, J., Yuan, H., Song, J., Qu, B., Xing, J., Wang, Q., Li, X., Duan, L., Li, N., & Wang, Y. (2021). Variation of Isoprenoid GDGTs in the Stratified Marine Water Column: Implications for GDGT-Based TEX86 Paleothermometry. *Frontiers in Marine Science*, *8*. https://doi.org/10.3389/fmars.2021.715708

Herbert, T. D. (2001). Review of alkenone calibrations (culture, water column, and sediments). *Geochemistry, Geophysics, Geosystems*, *2*(2), n/a-n/a. https://doi.org/10.1029/2000gc000055

Hernández-Sánchez, M., Woodward, E., Taylor, K., Henderson, G., & Pancost, R. (2014). Variations in GDGT distributions through the water column in the South East Atlantic Ocean. *Geochimica Et Cosmochimica Acta*, *132*, 337–348. https://doi.org/10.1016/j.gca.2014.02.009

Ho, S., Naafs, B., & Lamy, F. (2013). PALEOCEANOGRAPHY, BIOLOGICAL PROXIES | Alkenone Paleothermometry Based on the Haptophyte Algae. *Encyclopedia of Quaternary Science*, 755–764. https://doi.org/10.1016/b978-0-444-53643-3.00278-8

Huguet, C., Kim, J. H., Sinninghe Damsté, J. S., & Schouten, S. (2006). Reconstruction of sea surface temperature variations in the Arabian Sea over the last 23 kyr using organic proxies (TEX_{86} and $U^{K'}_{37}$). *Paleoceanography*, *21*(3). https://doi.org/10.1029/2005pa001215

Huguet, C., Schimmelmann, A., Thunell, R., Lourens, L. J., Sinninghe Damsté, J. S., & Schouten, S. (2007). A study of the TEX_{86} paleothermometer in the water column and sediments of the Santa Barbara Basin, California. *Paleoceanography*, *22*(3), n/a-n/a. https://doi.org/10.1029/2006pa001310

Hurley, S. J., Lipp, J. S., Close, H. G., Hinrichs, K. U., & Pearson, A. (2018). Distribution and export of isoprenoid tetraether lipids in suspended particulate matter from the water column of the Western Atlantic Ocean. *Organic Geochemistry*, *116*, 90–102. https://doi.org/10.1016/j.orggeochem.2017.11.010

Karner, M. B., DeLong, E. F., & Karl, D. M. (2001). Archaeal dominance in the mesopelagic zone of the Pacific Ocean. *Nature*, *409*(6819), 507–510. https://doi.org/10.1038/35054051

Kennedy, J. J., Rayner, N. A., Smith, R. O., Parker, D. E., & Saunby, M. (2011). Reassessing biases and other uncertainties in sea surface temperature observations measured in situ since 1850: 1. Measurement and sampling uncertainties. *Journal of Geophysical Research*, *116*(D14). https://doi.org/10.1029/2010jd015218

Kim, B., & Zhang, Y. G. (2022). Methane hydrate dissociation across the Oligocene–Miocene boundary. *Nature Geoscience*, *15*(3), 203–209. https://doi.org/10.1038/s41561-022-00895-5

Kim, J. H., Schouten, S., Rodrigo-Gámiz, M., Rampen, S., Marino, G., Huguet, C., Helmke, P., Buscail, R., Hopmans, E. C., Pross, J., Sangiorgi, F., Middelburg, J. B., & Sinninghe Damsté, J. S. (2015). Influence of deep-water derived isoprenoid tetraether lipids on the TEX86H paleothermometer in the Mediterranean Sea. *Geochimica Et Cosmochimica Acta*, *150*, 125–141. https://doi.org/10.1016/j.gca.2014.11.017

Kim, J. H., van der Meer, J., Schouten, S., Helmke, P., Willmott, V., Sangiorgi, F., Koç, N., Hopmans, E. C., & Damsté, J. S. S. (2010). New indices and calibrations derived from the distribution of crenarchaeal isoprenoid tetraether lipids: Implications for past sea surface temperature reconstructions. *Geochimica Et Cosmochimica Acta*, *74*(16), 4639–4654. https://doi.org/10.1016/j.gca.2010.05.027

Kim, J. H., Villanueva, L., Zell, C., & Sinninghe Damsté, J. S. (2016). Biological source and provenance of deep-water derived isoprenoid tetraether lipids along the Portuguese continental margin. *Geochimica Et Cosmochimica Acta*, *172*, 177–204. https://doi.org/10.1016/j.gca.2015.09.010

Könneke, M., Bernhard, A. E., de la Torre, J. R., Walker, C. B., Waterbury, J. B., & Stahl, D. A. (2005). Isolation of an autotrophic ammonia-oxidizing marine archaeon. *Nature*, *437*(7058), 543–546. https://doi.org/10.1038/nature03911

Kucera, M. (2019a). Determination of Past Sea Surface Temperatures. *Encyclopedia of Ocean Sciences*, 490–504. https://doi.org/10.1016/b978-0-12-409548-9.11384-3

Kucera, M. (2019b). Determination of Past Sea Surface Temperatures. *Encyclopedia of Ocean Sciences*, 490–504. https://doi.org/10.1016/b978-0-12-409548-9.11384-3

Laepple, T., & Huybers, P. (2014). Ocean surface temperature variability: Large model–data differences at decadal and longer periods. *Proceedings of the National Academy of Sciences*, *111*(47), 16682–16687. https://doi.org/10.1073/pnas.1412077111

Lawrence, K. T., Pearson, A., Castañeda, I. S., Ladlow, C., Peterson, L. C., & Lawrence, C. E. (2020). Comparison of Late Neogene $U^{k'}_{37}$ and TEX_{86} Paleotemperature Records From the Eastern Equatorial Pacific at Orbital Resolution. *Paleoceanography and Paleoclimatology*, *35*(7). https://doi.org/10.1029/2020pa003858

Malinverno, E. (2003). Coccolithophorid distribution in the Ionian Sea and its relationship to eastern Mediterranean circulation during late fall to early winter 1997. *Journal of Geophysical Research*, *108*(C9). https://doi.org/10.1029/2002jc001346

Malinverno, E., Triantaphyllou, M., Stavrakakis, S., Ziveri, P., & Lykousis, V. (2009). Seasonal and spatial variability of coccolithophore export production at the South-Western margin of Crete (Eastern Mediterranean). *Marine Micropaleontology*, *71*(3–4), 131–147. https://doi.org/10.1016/j.marmicro.2009.02.002

Millot, C., & Taupier-Letage, I. (2005). Circulation in the Mediterranean Sea. *The Mediterranean Sea*, 29–66. https://doi.org/10.1007/b107143

Mollenhauer, G., Basse, A., Kim, J. H., Sinninghe Damsté, J. S., & Fischer, G. (2015). A four-year record of U K′ 37 - and TEX 86 -derived sea surface temperature estimates from sinking particles in the filamentous upwelling region off Cape Blanc, Mauritania. *Deep Sea Research Part I: Oceanographic Research Papers*, *97*, 67–79. https://doi.org/10.1016/j.dsr.2014.11.015

Morcillo-Montalbá, L., Rodrigo-Gámiz, M., Martínez-Ruiz, F., Ortega-Huertas, M., Schouten, S., & Sinninghe Damsté, J. S. (2021). Rapid Climate Changes in the Westernmost Mediterranean (Alboran Sea) Over the Last 35 kyr: New Insights From Four Lipid Paleothermometers ($U^{K'}_{37}$, TEX^{H}_{86}, RI-OH', and LDI). *Paleoceanography and Paleoclimatology*, *36*(12). https://doi.org/10.1029/2020pa004171

Müller, P. J., Kirst, G., Ruhland, G., von Storch, I., & Rosell-Melé, A. (1998). Calibration of the alkenone paleotemperature index U37K′ based on core-tops from the eastern South Atlantic

and the global ocean (60°N-60°S). *Geochimica Et Cosmochimica Acta*, *62*(10), 1757–1772. https://doi.org/10.1016/s0016-7037(98)00097-0

O'Brien, C. L., Robinson, S. A., Pancost, R. D., Sinninghe Damsté, J. S., Schouten, S., Lunt, D. J., Alsenz, H., Bornemann, A., Bottini, C., Brassell, S. C., Farnsworth, A., Forster, A., Huber, B. T., Inglis, G. N., Jenkyns, H. C., Linnert, C., Littler, K., Markwick, P., McAnena, A., Wrobel, N. E. (2017). Cretaceous sea-surface temperature evolution: Constraints from TEX86 and planktonic foraminiferal oxygen isotopes. *Earth-Science Reviews*, *172*, 224–247. https://doi.org/10.1016/j.earscirev.2017.07.012

Park, E., Hefter, J., Fischer, G., Iversen, M. H., Ramondenc, S., Nöthig, E. M., & Mollenhauer, G. (2019). Seasonality of archaeal lipid flux and GDGT-based thermometry in sinking particles of high-latitude oceans: Fram Strait (79° N) and Antarctic Polar Front (50° S). *Biogeosciences*, *16*(11), 2247–2268. https://doi.org/10.5194/bg-16-2247-2019

Prahl, F. G., Muehlhausen, L. A., & Zahnle, D. L. (1988). Further evaluation of long-chain alkenones as indicators of paleoceanographic conditions. *Geochimica Et Cosmochimica Acta*, *52*(9), 2303–2310. https://doi.org/10.1016/0016-7037(88)90132-9

Prahl, F. G., & Wakeham, S. G. (1987). Calibration of unsaturation patterns in long-chain ketone compositions for palaeotemperature assessment. *Nature*, *330*(6146), 367–369. https://doi.org/10.1038/330367a0

Rattanasriampaipong, R., Zhang, Y. G., Pearson, A., Hedlund, B. P., & Zhang, S. (2022). Archaeal lipids trace ecology and evolution of marine ammonia-oxidizing archaea. *Proceedings of the National Academy of Sciences*, *119*(31). https://doi.org/10.1073/pnas.2123193119

Rice, A., Nooteboom, P. D., van Sebille, E., Peterse, F., Ziegler, M., & Sluijs, A. (2022). Limited Lateral Transport Bias During Export of Sea Surface Temperature Proxy Carriers in the Mediterranean Sea. *Geophysical Research Letters*, *49*(4). https://doi.org/10.1029/2021gl096859

Richey, J. N., & Tierney, J. E. (2016). GDGT and alkenone flux in the northern Gulf of Mexico: Implications for the TEX_{86} and $U^{K'}_{37}$ paleothermometers. *Paleoceanography*, *31*(12), 1547–1561. https://doi.org/10.1002/2016pa003032

Roether, W., Manca, B. B., Klein, B., Bregant, D., Georgopoulos, D., Beitzel, V., Kovačević, V., & Luchetta, A. (1996). Recent Changes in Eastern Mediterranean Deep Waters. *Science*, *271*(5247), 333–335. https://doi.org/10.1126/science.271.5247.333

Rosell-Melé, A., & Prahl, F. G. (2013). Seasonality of UK′37 temperature estimates as inferred from sediment trap data. *Quaternary Science Reviews*, *72*, 128–136. https://doi.org/10.1016/j.quascirev.2013.04.017

Roussenov, V., Stanev, E., Artale, V., & Pinardi, N. (1995). A seasonal model of the Mediterranean Sea general circulation. *Journal of Geophysical Research*, *100*(C7), 13515. https://doi.org/10.1029/95jc00233

Rutten, A., de Lange, G. J., Ziveri, P., Thomson, J., van Santvoort, P. J. M., Colley, S., & Corselli, C. (2000). Recent terrestrial and carbonate fluxes in the pelagic eastern Mediterranean; a comparison between sediment trap and surface sediment. *Palaeogeography, Palaeoclimatology, Palaeoecology*, *158*, 197–213.

Schouten, S., Hopmans, E. C., Schefuß, E., & Sinninghe Damsté, J. S. (2002). Distributional variations in marine crenarchaeotal membrane lipids: a new tool for reconstructing ancient sea water temperatures? *Earth and Planetary Science Letters*, *204*, 265–274.

Schouten, S., Hopmans, E. C., & Sinninghe Damsté, J. S. (2013). The organic geochemistry of glycerol dialkyl glycerol tetraether lipids: A review. *Organic Geochemistry*, *54*, 19–61. https://doi.org/10.1016/j.orggeochem.2012.09.006

Sicre, M. A., Ternois, Y., Miquel, J. C., & Marty, J. C. (1999). Alkenones in the northwestern Mediterranean Sea: Interannual variability and vertical transfer. *Geophysical Research Letters*, *26*(12), 1735–1738. https://doi.org/10.1029/1999gl900353

Sinninghe Damsté, J. S., Rijpstra, W. I. C., Hopmans, E. C., Jung, M. Y., Kim, J. G., Rhee, S. K., Stieglmeier, M., & Schleper, C. (2012). Intact Polar and Core Glycerol Dibiphytanyl Glycerol Tetraether Lipids of Group I.1a and I.1b Thaumarchaeota in Soil. *Applied and Environmental Microbiology*, *78*(19), 6866–6874. https://doi.org/10.1128/aem.01681-12

Skampa, E., Triantaphyllou, M., Dimiza, M., Gogou, A., Malinverno, E., Stavrakakis, S., Parinos, C., Panagiotopoulos, I., Tselenti, D., Archontikis, O., & Baumann, K. H. (2020). Coccolithophore export in three deep-sea sites of the Aegean and Ionian Seas (Eastern Mediterranean): Biogeographical patterns and biogenic carbonate fluxes. *Deep Sea Research Part II: Topical Studies in Oceanography*, *171*, 104690. https://doi.org/10.1016/j.dsr2.2019.104690

Taylor, K. W., Huber, M., Hollis, C. J., Hernandez-Sanchez, M. T., & Pancost, R. D. (2013). Re-evaluating modern and Palaeogene GDGT distributions: Implications for SST reconstructions. *Global and Planetary Change*, *108*, 158–174. https://doi.org/10.1016/j.gloplacha.2013.06.011

Techtmann, S. M., Fortney, J. L., Ayers, K. A., Joyner, D. C., Linley, T. D., Pfiffner, S. M., & Hazen, T. C. (2015). The Unique Chemistry of Eastern Mediterranean Water Masses Selects for Distinct Microbial Communities by Depth. *PLOS ONE*, *10*(3), e0120605. https://doi.org/10.1371/journal.pone.0120605

Tennant, D. A., & Baker, E. T. (1992). A fast, high-precision splitter for particle suspensions. *Marine Geology*, *108*(3–4), 247–252. https://doi.org/10.1016/0025-3227(92)90198-q

Ternois, Y., Sicre, M. A., Boireau, A., Conte, M., & E, G. (1997). Evaluation of long-chain alkenones as paleo-temperature indicators in the Mediterranean Sea. *Deep Sea Research Part I: Oceanographic Research Papers*, *44*(2), 271–286. https://doi.org/10.1016/s0967-0637(97)89915-3

Ternois, Y., Sicre, M. A., Boireau, A., Marty, J. C., & Miquel, J. C. (1996). Production pattern of alkenones in the Mediterranean Sea. *Geophysical Research Letters*, *23*(22), 3171–3174. https://doi.org/10.1029/96gl02910

Tierney, J. E., & Tingley, M. P. (2014). A Bayesian, spatially-varying calibration model for the TEX86 proxy. *Geochimica Et Cosmochimica Acta*, *127*, 83–106. https://doi.org/10.1016/j.gca.2013.11.026

Tierney, J. E., & Tingley, M. P. (2018). BAYSPLINE: A New Calibration for the Alkenone Paleothermometer. *Paleoceanography and Paleoclimatology*, *33*(3), 281–301. https://doi.org/10.1002/2017pa003201

Triantaphyllou, M., Dimiza, M., Krasakopoulou, E., Malinverno, E., Lianou, V., & Souvermezoglou, E. (2010). Seasonal variation in Emiliania huxleyi coccolith morphology and calcification in the Aegean Sea (Eastern Mediterranean). *Geobios*, *43*(1), 99–110. https://doi.org/10.1016/j.geobios.2009.09.002

Triantaphyllou, M. V. (2004). Coccolithophore export production and response to seasonal surface water variability in the oligotrophic Cretan Sea (NE Mediterranean). *Micropaleontology*, *50*(Suppl_1), 127–144. https://doi.org/10.2113/50.suppl_1.127

van der Weijst, C. M. H., van der Laan, K. J., Peterse, F., Reichart, G. J., Sangiorgi, F., Schouten, S., Veenstra, T. J. T., & Sluijs, A. (2022). A 15-million-year surface- and subsurface-integrated TEX_{86} temperature record from the eastern equatorial Atlantic. *Climate of the Past*, *18*(8), 1947–1962. https://doi.org/10.5194/cp-18-1947-2022

Warren, J. (2018). Deepsea Hypersaline Anoxic Lakes & Basins (DHALs & DHABS). *Salty Matters*.

Wei, B., Jia, G., Hefter, J., Kang, M., Park, E., Wang, S., & Mollenhauer, G. (2020). Comparison of the Uk'37, LDI, TEXH86, and RI-OH temperature proxies in sediments from the northern shelf of the South China Sea. *Biogeosciences, 17*, 4489-4508. https://doi.org/10.5194/bg-17-4489-2020

Weijers, J. W., Schouten, S., Spaargaren, O. C., & Sinninghe Damsté, J. S. (2006). Occurrence and distribution of tetraether membrane lipids in soils: Implications for the use of the TEX86 proxy and the BIT index. *Organic Geochemistry*, *37*(12), 1680–1693. https://doi.org/10.1016/j.orggeochem.2006.07.018

Wuchter, C., Schouten, S., Wakeham, S. G., & Sinninghe Damsté, J. S. (2006). Archaeal tetraether membrane lipid fluxes in the northeastern Pacific and the Arabian Sea: Implications for TEX_{86} paleothermometry. *Paleoceanography*, *21*(4). https://doi.org/10.1029/2006pa001279

Zavatarelli, M., & Mellor, G. L. (1994). A Numerical Study of the Mediterranean Sea Circulation. *Journal of Physical Oceanography*, *25*(6), 1384–1414. https://doi.org/10.1175/1520-0485(1995)025

Zhang, T., Xiao, X., Chen, S., Zhao, J., Chen, Z., Feng, J., Liang, Q., Phelps, T. J., & Zhang, C. (2020). Active Anaerobic Archaeal Methanotrophs in Recently Emerged Cold Seeps of Northern South China Sea. *Frontiers in Microbiology*, *11*. https://doi.org/10.3389/fmicb.2020.612135

Ziveri, P., Grandi, C., Stefanetti, A., & Cita, M. B. (1995). Biogenic fluxes in Bannock Basin: first results from a sediment trap study (November 1991 - May 1992). *Rendiconti Lincei*, *6*(2), 131–145. https://doi.org/10.1007/bf03001662

Ziveri, P., Rutten, A., de Lange, G. J., Thomson, J., & Corselli, C. (2000). Present-day coccolith fluxes recorded in central eastern Mediterranean sediment traps and surface sediments. *Palaeogeography, Palaeoclimatology, Palaeoecology*, *158*, 175–195.

Appendix 1. $U^{k'}_{37}$ values and TEX_{86} values

Table 2. $U^{k'}_{37}$ values, $U^{k'}_{37}$ estimates, and flux weighted average at the three trap deployment depths.

	500 m trap		1500 m trap		2500 m trap	
	$U^{k'}_{37}$	$U^{k'}_{37}$ SST (ºC)	$U^{k'}_{37}$	$U^{k'}_{37}$ SST (ºC)	$U^{k'}_{37}$	$U^{k'}_{37}$ SST (ºC)
2008						
NOV	BDL	BDL	BDL	BDL	0.70	19.3
DEC	BDL	BDL	0.72	19.9	0.69	19.3
2009						
JAN	0.69	19.0	BDL	BDL	0.68	18.7
FEB	0.79	22.1	0.42	11.2	0.63	17.2
	0.88	24.8	0.60	16.5	0.54	14.7
MAR	0.96	27.2	0.54	14.7	BDL	BDL
APR	0.98	27.6	0.44	11.9	0.46	12.3
	0.91	25.6	0.44	11.8	BDL	BDL
MAY	0.85	23.8	0.19	4.4	0.46	12.4
JUN	BDL	BDL	0.46	12.3	0.53	14.4
JUL	0.89	25.1	0.49	13.2	0.50	13.6
	0.81	22.8	0.46	12.4	0.48	13.1
AUG	0.59	16.3	0.56	15.5	BDL	BDL
SEP	0.71	19.7	0.67	18.6	0.33	8.7
OKT	0.76	21.1	0.54	14.7	0.80	22.5
	0.76	21.3	0.74	20.6	BDL	BDL
NOV	0.72	20.2	0.76	21.2	BDL	BDL
DEC	0.60	16.5	0.43	11.5	0.65	17.9
2010						
JAN	0.57	15.7	BDL	BDL	BDL	BDL
	0.46	12.5	0.62	17.1	0.59	16.2
FEB	0.46	12.5	ND	ND	0.53	14.3
MAR	0.46	12.2	0.42	11.1	0.55	15.1
APR	0.43	11.4	0.62	17.2	0.46	12.5
	0.43	11.6	0.51	13.9	0.47	12.5
MAY	0.47	12.6	0.56	15.3	0.57	15.6
JUN	0.49	13.4	0.55	14.9	0.63	17.3
	0.51	13.7	0.64	17.6	BDL	BDL
JUL	0.58	16.0	0.60	16.6	BDL	BDL
AUG	0.66	18.1	0.60	16.5	BDL	BDL
	0.66	18.3	0.74	20.7	BDL	BDL
SEP	0.73	20.4	0.78	21.9	BDL	BDL
OKT	0.69	19.3	0.74	20.7	BDL	BDL
	0.67	18.7	0.82	22.8	BDL	BDL
NOV	0.65	18.0	0.82	23.0	BDL	BDL
DEC	0.64	17.5	1.00	28.3	BDL	BDL
	0.58	15.8	BDL	BDL	BDL	BDL
2011						
JAN	0.55	14.9	0.70	19.4	0.20	4.6
FEB	0.58	15.8	0.70	19.3	0.32	8.4
MAR	0.55	15.0	0.65	18.0	0.39	10.3
	0.48	13.0	BDL	BDL	0.47	12.7
APR	0.46	12.4	0.56	15.2	0.50	13.5
FWA[1]	0.62	17.1	0.55	15.1	0.55	15.1

[1] Flux Weighted Average. BDL = Below detection level

Table 3. TEX_{86} values, TEX_{86} estimates, and flux weighted average at the three trap deployment depths.

	500 m trap		1500 m trap		2500 m trap	
	TEX^{H}_{86}	TEX^{H}_{86} SST (ºC)	TEX^{H}_{86}	TEX^{H}_{86} SST (ºC)	TEX^{H}_{86}	TEX^{H}_{86} SST (ºC)
2008						
NOV	-0.13	29.7	-0.13	30.0	-0.12	30.6
DEC	BDL	BDL	-0.12	30.2	-0.11	31.0
2009						
JAN	-0.12	30.4	-0.13	29.6	-0.12	30.6
FEB	-0.12	30.6	-0.11	30.8	-0.12	30.4
	-0.12	30.1	-0.12	30.2	-0.12	30.4
MAR	-0.15	28.3	-0.12	30.4	-0.13	29.4
APR	-0.13	29.5	-0.13	29.8	-0.13	29.9
	-0.15	28.3	-0.14	29.3	-0.12	30.2
MAY	-0.15	28.4	-0.14	29.0	-0.13	29.7
JUN	ND	ND	-0.15	28.2	-0.13	29.5
JUL	-0.15	28.1	-0.16	27.8	-0.14	29.2
	-0.15	28.4	-0.13	29.6	-0.14	29.0
AUG	-0.14	29.3	-0.13	29.5	-0.15	28.6
SEP	-0.14	29.4	-0.15	28.6	-0.14	29.1
OKT	-0.14	29.1	-0.15	28.3	-0.17	27.3
	-0.14	28.9	-0.12	30.3	-0.14	29.1
NOV	-0.14	28.9	-0.12	30.4	-0.13	29.5
DEC	-0.12	30.4	-0.12	30.2	-0.12	30.7
2010						
JAN	-0.13	30.0	-0.13	30.1	-0.14	29.1
	-0.12	30.4	-0.12	30.6	-0.12	30.6
FEB	-0.13	29.9	BDL	BDL	-0.12	30.4
MAR	-0.12	30.2	-0.13	29.6	-0.12	30.5
APR	BDL	BDL	-0.15	28.5	-0.12	30.3
	-0.14	28.7	-0.16	27.5	-0.13	29.6
MAY	-0.14	29.3	-0.14	29.0	-0.12	30.6
JUN	-0.13	29.6	-0.13	29.4	-0.12	30.3
	-0.13	29.7	-0.14	28.9	-0.12	30.4
JUL	-0.13	29.7	-0.14	29.2	-0.13	29.9
AUG	-0.13	29.6	-0.13	29.7	-0.13	29.5
	-0.13	29.7	-0.14	29.4	-0.13	30.1
SEP	-0.13	29.9	-0.13	29.6	-0.13	29.9
OKT	-0.13	29.6	-0.12	30.2	-0.18	26.3
	-0.13	29.7	-0.14	28.9	-0.14	28.8
NOV	-0.13	29.5	-0.15	28.2	-0.14	28.9
DEC	-0.13	29.6	-0.14	29.0	-0.14	29.1
	-0.13	29.7	-0.13	29.4	-0.14	29.2
2011						
JAN	-0.13	29.6	-0.13	30.1	-0.14	29.2
FEB	-0.13	29.8	-0.14	28.7	-0.14	28.9
MAR	-0.13	30.0	-0.14	29.4	-0.13	29.8
	-0.13	30.0	-0.13	29.5	-0.12	30.3
APR	-0.13	29.8	-0.14	29.0	-0.12	30.3
FWA[1]	-0.14	29.4	-0.13	29.7	-0.12	30.2

[1] Flux Weighted Average. BDL = Below detection level

Appendix 2. IsoGDGT values at the three depths

Table 4. IsoGDGT ratios at 500 m depth.

	[GDGT-2]/[GDGT-3]	[GDGT-0]/[Cren]	[Cren']/([Cren] + [Cren'])
2008			
NOV	16.28	0.37	0.11
DEC	BDL	BDL	BDL
2009			
JAN	19.39	0.32	0.11
FEB	19.21	0.34	0.11
	17.24	0.33	0.10
MAR	9.43	0.40	0.09
APR	10.74	0.40	0.10
	9.68	0.38	0.09
MAY	8.93	0.41	0.08
JUN	BDL	BDL	BDL
JUL	10.02	0.39	0.09
	10.55	0.38	0.09
AUG	11.69	0.36	0.08
SEP	12.44	0.38	0.09
OKT	11.50	0.38	0.09
	11.71	0.40	0.09
NOV	12.30	0.40	0.09
DEC	19.35	0.36	0.10
2010			
JAN	18.84	0.34	0.10
	18.76	0.33	0.10
FEB	15.80	0.33	0.10
MAR	14.79	0.35	0.11
APR	BDL	BDL	BDL
	9.96	0.40	0.08
MAY	11.07	0.38	0.09
JUN	11.57	0.36	0.09
	12.36	0.36	0.10
JUL	12.55	0.33	0.10
AUG	13.08	0.34	0.09
	14.34	0.35	0.09
SEP	13.84	0.35	0.10
OKT	13.80	0.35	0.09
	13.95	0.36	0.09
NOV	14.79	0.37	0.09
DEC	15.23	0.37	0.09
	14.41	0.37	0.09
2011			
JAN	14.79	0.36	0.09
FEB	15.60	0.37	0.10
MAR	15.62	0.36	0.09
	15.24	0.35	0.10
APR	16.87	0.35	0.10

Table 5. IsoGDGT ratios at 1500 m depth.

	[GDGT-2]/[GDGT-3]	[GDGT-0]/[Cren]	[Cren']/([Cren] + [Cren'])
2008			
NOV	16.30	0.35	0.10
DEC	18.85	0.35	0.10
2009			
JAN	10.60	0.47	0.12
FEB	13.96	0.33	0.11
	15.35	0.34	0.10
MAR	15.59	0.33	0.10
APR	11.33	0.36	0.10
	10.31	0.38	0.09
MAY	10.86	0.38	0.09
JUN	8.97	0.40	0.08
JUL	11.43	0.49	0.08
	11.47	0.37	0.10
AUG	11.76	0.36	0.09
SEP	12.10	0.44	0.09
OKT	12.66	0.39	0.09
	17.65	0.36	0.10
NOV	18.51	0.34	0.10
DEC	21.13	0.35	0.10
2010			
JAN	19.09	0.35	0.10
	18.76	0.32	0.10
FEB	BDL	BDL	BDL
MAR	15.25	0.36	0.09
APR	8.96	0.41	0.09
	8.95	0.43	0.07
MAY	13.27	0.37	0.09
JUN	12.36	0.38	0.09
	12.23	0.38	0.08
JUL	13.68	0.37	0.09
AUG	14.99	0.36	0.09
	14.60	0.38	0.09
SEP	15.31	0.34	0.09
OKT	17.62	0.33	0.11
	15.08	0.41	0.09
NOV	13.68	0.46	0.08
DEC	14.22	0.48	0.09
	13.98	0.53	0.10
2011			
JAN	18.89	0.37	0.10
FEB	14.19	0.44	0.09
MAR	16.17	0.43	0.08
	14.02	0.40	0.09
APR	13.12	0.41	0.09

Table 6. IsoGDGT ratios at 2500 m depth.

	[GDGT-2]/[GDGT-3]	[GDGT-0]/[Cren]	[Cren']/([Cren] + [Cren'])
2008			
NOV	17.74	0.32	0.11
DEC	19.05	0.32	0.12
2009			
JAN	16.15	0.33	0.11
FEB	16.48	0.32	0.10
	15.97	0.33	0.10
MAR	11.19	0.41	0.10
APR	13.48	0.39	0.10
	12.19	0.38	0.10
MAY	13.78	0.43	0.09
JUN	12.81	0.39	0.09
JUL	12.28	0.41	0.09
	12.85	0.46	0.08
AUG	11.20	0.46	0.09
SEP	12.01	0.46	0.08
OKT	9.10	0.46	0.08
	11.00	0.44	0.10
NOV	13.77	0.40	0.10
DEC	18.94	0.33	0.10
2010			
JAN	11.41	0.56	0.09
	19.37	0.37	0.10
FEB	16.49	0.35	0.10
MAR	15.68	0.35	0.10
APR	14.41	0.35	0.10
	10.21	0.37	0.10
MAY	13.44	0.36	0.10
JUN	14.47	0.33	0.10
	15.22	0.34	0.10
JUL	13.68	0.37	0.09
AUG	14.10	0.46	0.09
	15.25	0.38	0.10
SEP	15.56	0.44	0.09
OKT	13.69	0.60	0.08
NOV	13.90	0.61	0.08
DEC	14.17	0.56	0.09
	12.84	0.58	0.08
2011			
JAN	12.92	0.51	0.09
FEB	11.95	0.55	0.08
MAR	15.06	0.42	0.09
	15.43	0.44	0.09
APR	15.79	0.37	0.09

Appendix 3. P and R^2 values

Table 7. P values: pairwise comparison between [GDGT-2]/[GDGT-3] ratio, [GDGT-0]/Cren ratio, [Cren']/(Cren + [Cren']) ratio and TEX_{86} SST within each trap deployment depth (dark). P < 0.005 (bold).

		500 m				1500 m				2500 m			
		[GDGT-2]/[GDGT-3]	[GDGT-0]/Cren	[Cren']/([Cren]+[Cren'])	TEX_{86} SST	[GDGT-2]/[GDGT-3]	[GDGT-0]/Cren	[Cren']/([Cren]+[Cren'])	TEX_{86} SST	[GDGT-2]/[GDGT-3]	[GDGT-0]/Cren	[Cren']/([Cren]+[Cren'])	TEX_{86} SST
500 m	[GDGT-2]/[GDGT-3]		0	0.168	**$2.22E^{-16}$**	0.460	0.696	0.020	0.090	0.603	0.914	0.251	0.669
	[GDGT-0]/Cren	0		0.489	**$3.89E^{-14}$**	0.992	0.656	0.249	0.331	0.564	0.469	0.121	0.246
	[Cren']/(Cren+[Cren'])	**$2.22E^{-16}$**	**$3.89E^{-14}$**		0.012	0.273	0.872	0.018	0.082	0.604	0.973	0.140	0.539
	TEX_{86} SST	0.168	0.489	0.012		0.002	0.337	0.002	0.011	0.463	0.900	0.070	0.451
1500 m	[GDGT-2]/[GDGT-3]	0.460	0.992	0.002	0.273		**0.003**	**0.005**	**$4.74E^{-07}$**	0.059	0.443	0.478	0.825
	[GDGT-0]/Cren	0.696	0.656	0.337	0.872	**0.003**		0.015	**$9.71E^{-07}$**	0.181	0.010	0.006	0.045
	[Cren']/(Cren+[Cren'])	0.090	0.331	0.011	0.082	**$4.74E^{-07}$**	**$9.71E^{-07}$**		**$1.35E^{-10}$**	0.016	0.180	0.007	0.040
	TEX_{86} SST	0.020	0.249	0.002	0.018	**0.005**	0.015	**$1.35E^{-10}$**		0.040	0.197	0.006	0.111
2500 m	[GDGT-2]/[GDGT-3]	0.603	0.564	0.463	0.604	0.059	0.181	0.040	0.016		**0.001**	**$7.24E^{-05}$**	**$9.67E^{-10}$**
	[GDGT-0]/Cren	0.914	0.469	0.900	0.973	0.443	0.010	0.197	0.180	**0.001**		**$8.19E^{-11}$**	**$2.51E^{-08}$**
	[Cren']/(Cren+[Cren'])	0.669	0.246	0.451	0.539	0.825	0.045	0.111	0.040	**$9.67E^{-10}$**	**$2.51E^{-08}$**		**$1.15E^{-10}$**
	TEX_{86} SST	0.251	0.121	0.070	0.140	0.478	0.006	0.006	0.007	**$7.24E^{-05}$**	**$8.19E^{-11}$**	**$1.15E^{-10}$**	

Table 8. R^2 values: pairwise comparison between [GDGT-2]/[GDGT-3] ratio, [GDGT-0]/Cren ratio, [Cren']/(Cren + [Cren']) ratio and TEX_{86} SST within each trap deployment depth (dark). P < 0.005 (bold).

		500 m				1500 m				2500 m			
		[GDGT-2]/[GDGT-3]	[GDGT-0]/Cren	[Cren']/([Cren]+[Cren'])	TEX_{86} SST	[GDGT-2]/[GDGT-3]	[GDGT-0]/Cren	[Cren']/([Cren]+[Cren'])	TEX_{86} SST	[GDGT-2]/[GDGT-3]	[GDGT-0]/Cren	[Cren']/([Cren]+[Cren'])	TEX_{86} SST
500 m	[GDGT-2]/[GDGT-3]		0.858	0.052	**0.849**	0.015	0.004	0.141	0.078	0.008	0.000	0.036	0.005
	[GDGT-0]/Cren	0.858		0.013	**0.800**	0.000	0.006	0.037	0.026	0.009	0.015	0.066	0.037
	[Cren']/(Cren+[Cren'])	**0.849**	**0.800**		0.162	0.033	0.001	0.147	0.082	0.008	0.000	0.060	0.011
	TEX_{86} SST	0.052	0.013	0.162		0.237	0.026	0.229	0.165	0.015	0.000	0.089	0.016
1500 m	[GDGT-2]/[GDGT-3]	0.015	0.000	0.237	0.033		**0.202**	**0.187**	**0.482**	0.088	0.015	0.013	0.001
	[GDGT-0]/Cren	0.004	0.006	0.026	0.001	**0.202**		0.142	**0.463**	0.045	0.159	0.179	0.099
	[Cren']/(Cren+[Cren'])	0.078	0.026	0.165	0.082	**0.482**	**0.463**		**0.657**	0.140	0.046	0.174	0.104
	TEX_{86} SST	0.141	0.037	0.229	0.147	**0.187**	0.142	**0.657**		0.103	0.042	0.177	0.064
2500 m	[GDGT-2]/[GDGT-3]	0.008	0.009	0.015	0.008	0.088	0.045	0.103	0.140		**0.236**	**0.343**	**0.631**
	[GDGT-0]/Cren	0.000	0.015	0.000	0.000	0.015	0.159	0.042	0.046	**0.236**		**0.675**	**0.563**
	[Cren']/(Cren+[Cren'])	0.005	0.037	0.016	0.011	0.001	0.099	0.064	0.104	**0.631**	**0.563**		**0.699**
	TEX_{86} SST	0.036	0.066	0.089	0.060	0.013	0.179	0.177	0.174	**0.343**	**0.675**	**0.699**	